Engineering Structures 291 (2023) 116388

Contents lists available at ScienceDirect

Engineering Structures

journal homepage: www.elsevier.com/locate/engstruct

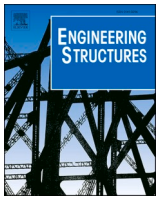

Low lateral stiffness underground structures for improved seismic performance. Application to the Kobe Daikai station

Xiangbo Bu [a], Alberto Ledesma [b], Francisco López-Almansa [c,*]

[a] Universitat Politècnica de Catalunya - BarcelonaTech (UPC), Civil and Environmental Eng. Department, UPC Campus Nord, 08034 Barcelona, Spain
[b] Universitat Politècnica de Catalunya - BarcelonaTech (UPC), Civil and Environmental Eng. Department and Center for Numerical Methods in Engineering - CIMNE, UPC Campus Nord, 08034 Barcelona, Spain
[c] Universitat Politècnica de Catalunya - BarcelonaTech (UPC), Architecture Technology Department, UPC Campus Nord, 08034 Barcelona, Spain currently Associate Researcher Natural and Anthropogenic Risks Research Center, Univ. Austral de Chile, Valdivia, Chile

ARTICLE INFO

Keywords:
Cut-and-cover underground structures
Subway and railway stations
Concrete hinged and sliding connections
Earthquake damage
Kobe earthquake
Daikai Station

ABSTRACT

Underground cut-and-cover structures are commonly designed as rigid box sections; however, in practical applications, connections between walls and slabs are frequently rather hinged (because of ease of construction). The abovementioned rigid configurations are highly sensitive to seismic ground motions, due to their important lateral stiffness and internal hyperstaticity; conversely, structures with articulated (or sliding) members have a smaller lateral stiffness, and would be significantly less affected by seismic waves, as would simply accommodate the imposed strains. This flexible solution has been widely considered in practice, but has received little attention from the academic community; this paper tries to close this gap by investigating preliminarily the seismic performance of box-section underground structures with hinged or sliding members. The well-known Daikai Station, damaged by the 1995 Kobe earthquake is analyzed in this paper as a highly relevant case study. An alternative solution is proposed for that station; both simplified and precise calculations have been performed. The simplified calculations are linear static analyses of the station-soil system; the soil-structure interaction is represented by a simple classical model. The precise calculations are nonlinear time-history analyses of an integrated finite element model of the station and the surrounding soil. Both types of analyses refer to the traditional and the proposed solutions of the station. The results of the static and dynamic analyses are satisfactorily compared; they prove that the proposed flexible solution is fully feasible and provides better seismic performance. Finally, another paper by the same authors presented a supplementary case study on a 2-story 3-bay subway station; the outcomes of these two studies could contribute to ground this constructive solution for shallow underground rectangular cut-and-cover structures in seismic areas (both for new construction and retrofit). Noticeably, this approach can be utilized for both cast-in-place and precast structures.

1. Introduction

Underground structures for road and railway infrastructure are being constructed worldwide at an increasing rate due to the gradual saturation of space above ground, especially in densely populated and built-up urban areas [1]. More precisely, according to the International Association of Public Transport [2], some 5400 km metro lines are under construction or in testing phases, and another 1700 km in design and tender stages. However, during the initial development of the underground structures, seismic issues did not receive enough attention [3]. In this sense, it is generally believed that such constructions are constrained by the surrounding medium, and the structure own inertial effect is of little importance; therefore, the seismic performance of underground structures should be better than that of aboveground structures. Despite this being generally true, not all the buried constructions are totally invulnerable to seismic events [4,5]; more precisely, bored and mined deep tunnels (circular and horseshoe-shaped, apart from other more irregular sections) are rather insensitive to seismic ground motions (except some particular situations, such as tunnel portals, faults-crossing, soil liquefaction, irregular soil, high curvature, intersection with lateral galleries or ventilation and evacuation shafts, among others), while shallow cut-and-cover (rectangular) road and railway tunnels and stations are more intensely affected by earthquakes. This difference is contributed by several reasons: (i) cut-and-cover tunnels

* Corresponding author.
E-mail addresses: xiangbo.bu@upc.edu (X. Bu), alberto.ledesma@upc.edu (A. Ledesma), francesc.lopez-almansa@upc.edu (F. López-Almansa).

https://doi.org/10.1016/j.engstruct.2023.116388
Received 30 January 2023; Received in revised form 27 April 2023; Accepted 27 May 2023
Available online 9 June 2023

are commonly shallower, thus undergoing stronger soil shakes, (ii) in cut-and-cover tunnels, the soil is ordinarily softer, this generating also more intense ground motions, (iii) the linings of circular, horseshoe and irregular section-tunnels are rather slender and, thus, can adapt to the ground-imposed displacements without high internal strains, and (iv) occasionally such linings are made of partially-hinged dowels (circumferential and longitudinal joints of segmental tunnel lining, mainly in circular sections) thus being even more distortion-insensitive.

Conversely to the lining flexibility of circular-like tunnels, rectangular tunnel and station structures are commonly statically redundant (hyperstatic) and highly robust (stiff) moment-resisting frames; therefore, they are generally unable to accommodate the seismic-generated racking motions without relevant internal strains [6,7]. Fig. 1.a presents a sketch of a cross-section of a typical two-story rectangular station, and Fig. 1.b displays its racking deformation during a strong earthquake.

Fig. 1.b shows that the soil deformation generates relevant strains into the structural members; given that the seismic events are basically indirect actions (i.e. imposed displacements), the stiffening and strengthening of the frame will not alleviate this situation, but rather causing the opposite effect. This last consideration highlights the practical impossibility of designing rigid box sections that are able to resist extremely strong ground motions without severe damage (mainly in rigid soils, as they do not yield, even to the determined opposition of the structure).

Various strategies have been proposed to upgrade the seismic performance of shallow cut-and-cover underground structures. First, seismic isolation layers featured with rubber, foam or other geotechnical materials are expected to weaken the constraint of the site soil [8–10]. Second, central columns are the most vulnerable elements; therefore, the release of binding at their ends reduces their internal forces while maintains sufficient load-bearing capacity. Flexible joints, such as rubber bearings [11], shear panel dampers [12] and friction pendulum bearings [13] have been proposed.

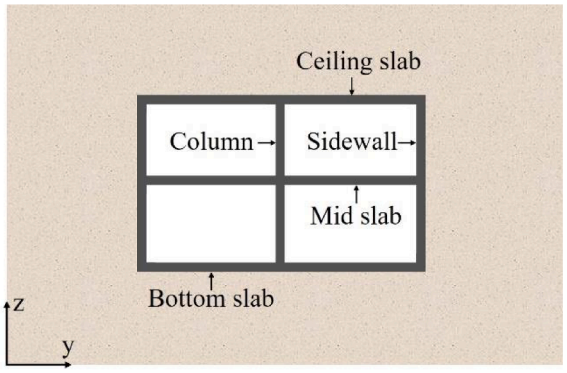

(a) Typical section of a cut-and-cover underground station

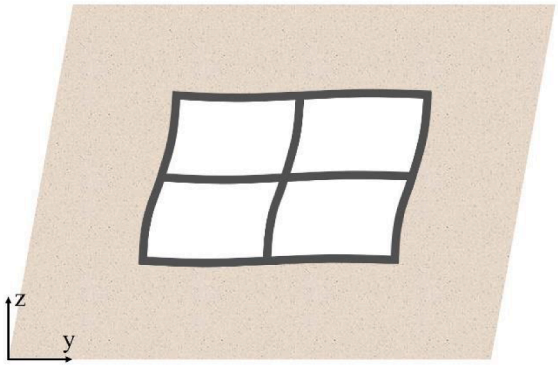

(b) Seismic behavior of the conventional moment-resisting frame

Fig. 1. Traditional rigid box section for shallow underground structures.

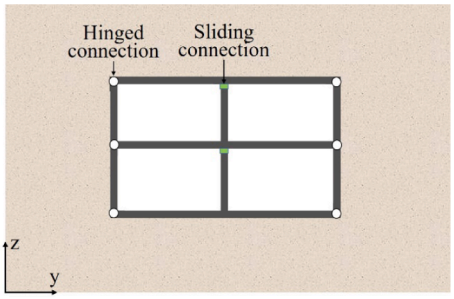

(a) Proposed hinged-sliding solution

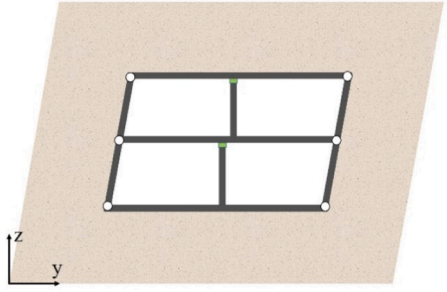

(b) Seismic behavior of the proposed hinged-sliding solution

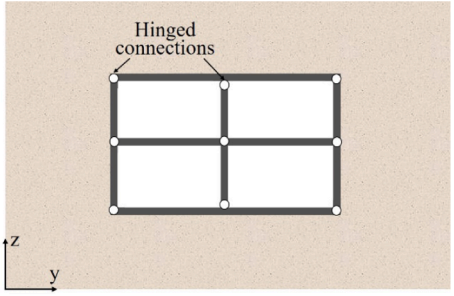

(c) Proposed hinged solution

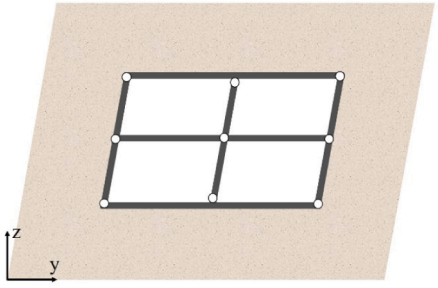

(d) Seismic behavior of the proposed hinged solution

Fig. 2. Proposed alternative solution for shallow underground structures.

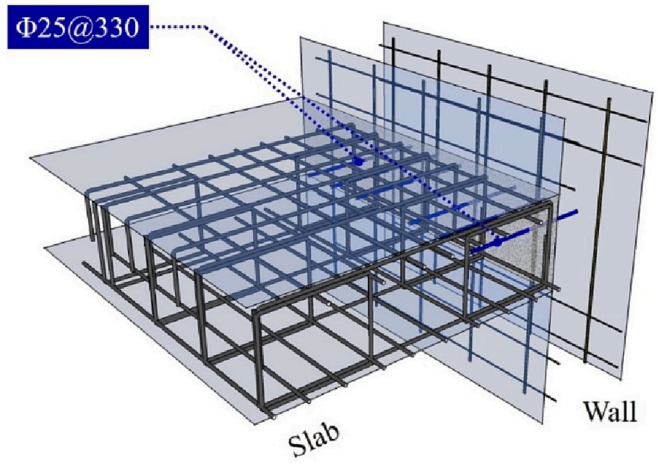

Fig. 3. Example of rather hinged connection in a cast-in-situ station of the high speed train Barcelona-Paris (Girona, 100 km north of Barcelona). Units in mm.

2. Proposed new "low lateral stiffness solution" for shallow underground structures

This paper proposes an opposite alternative solution to the traditional approach in Fig. 1; that solution consists in lessening the resistance to the imposed seismic racking, by designing a frame with low lateral stiffness; two possible versions of this solution are depicted by Fig. 2.a and Fig. 2.c. Fig. 2.a shows that the rigid connections between walls and slabs have been replaced with hinges, and the column-slab connections are sliding; similarly, in Fig. 2.c all the connections are hinged. Fig. 2.b and Fig. 2.d describe how the imposed racking deformation does not generate any relevant strain in the frame. Noticeably, the central columns, being the most commonly damaged structural elements in conventional underground structures (Fig. 5.c), undergo only a vertically centered load; therefore, in such element, the risk of buckling (2^{nd} order effects) and the expected damage are severely diminished. Finally, the effects of the vertical seismic ground motion are not significantly affected by the proposed solution.

The proposed alternative solutions described in Fig. 2.a and Fig. 2.c cannot be considered as totally ground-breaking, as they are merely adaptations of traditional approaches used to absorb imposed displacements. In this sense, the well-known quote by the Chinese philosopher Confucius "*The green reed which bends in the wind is stronger than the mighty oak which breaks in a storm*" applies. Another proof that this idea is not completely new is that the well-known report [14] states that, from the seismic design standpoint, it is desirable to make the structure flexible rather than to stiffen it. Noticeably, the paper [15] mentions that the proportion of damaged cases for the lined tunnels appears to be greater than that for the unlined cases; however, the authors attributed this phenomenon to the poor ground conditions that originally required the openings to be lined. Also, [16] offered two other possible explanations: (i) damage in the form of cracking or spalling is easier to identify in lined cases, and (ii) lined openings are more likely to be classified as damaged because of their high cost and importance. Without denying the plausibility of these considerations, another credible interpretation is that the lining stiffness is the problem, rather than the solution. Another proof that the proposed approach is not totally new, is that tunnels crossing active faults frequently incorporate flexible transverse joints to accommodate the fault displacements [17,18].

Broadly speaking, three major objections might be posed to the proposed alternative solution: amplification of the second order (P-Delta) effects, larger residual lateral displacements, and loss of sealing. Brief discussions on these issues are included next.

- **Amplification of the P-Delta effects**. Larger maximum lateral (racking) seismic displacements (compared to traditional solutions with rigid connections) are to be expected; for instance, [14] states that the maximum displacement of a station with zero lateral stiffness (similar to those in Fig. 2.a and Fig. 2.c) is approximately two times that of a station whose lateral stiffness is similar to that of the soil (Fig. 1.a). Regarding the Daikai station, similar remarks are obtained (sections 5 and 8); however, the second-order bending moments generated in the side walls by these larger displacements are irrelevant compared to the first-order values. The study [24] provides analogous conclusions. These considerations highlight the generalizability of this trend to other underground constructions. Finally, these larger maximum displacements can be absorbed by the mechanical and electrical installations; however, they need to be taken into consideration in their design.
- **Larger residual displacements**. Although the previous paragraph shows that the maximum drift displacements are larger for the proposed structures with low lateral stiffness, the situation for the residual (permanent) displacements is totally different. Regarding Daikai station, section 8 shows that the relation between the permanent displacements is totally random; more precisely, in most of the cases the largest permanent drift corresponds to the traditional solution (Fig. 1.a). This trend is corroborated with the numerical study in [54] and shaking table test in [6].
- **Loss of sealing**. The sealing effect is guaranteed by the water proofing system (subsection 4.3).

Finally, perhaps the most convincing corroboration of the proposed technology feasibility is that, although cut-and-cover cast-in-situ underground structures are commonly designed with rigid box sections, are frequently built as hinged, mostly for ease of construction. In this context, Fig. 3 displays a connection between a wall and a slab of the Girona underground station of a high speed train (Barcelona-Paris railway line); the overall structural configuration of this station is close to that of Fig. 2.a and Fig. 2.c.

Fig. 3 shows that the connection displayed consists of a suite of 25 mm diameter horizontal steel bars separated 33 cm; these bars are resin-coated to increase bonding. As mentioned before, this solution is utilized because of construction simplicity; the wall is cast first, the steel bars are inserted later on it (leaving a protruding segment to be embedded within the slab), and finally the slab is cast. The objective of this reinforcement is to resist the vertical shear force (can be considered as a kind of steel shear key, then); as the bars are located at the slab section center line, the bending resistance of this connection is rather low, being close to a true hinge. Other similar cases have been found in the metro lines of Panama city, Lima and Quito [19]; presumably, this construction detail is quite frequent, given its abovementioned ease of construction.

Despite the flexible solution depicted in Fig. 3 has been widely considered in practical applications worldwide, it has received little attention from the academic community; this paper tries to close this gap (and going further) by investigating preliminarily the seismic performance of box-section underground structures with hinged or sliding members (walls, slabs and columns), as the solutions described in Fig. 2.a and Fig. 2.c. In other words, the rather hinged solution adopted for easiness, might provide a better seismic capacity than the conventional one (rigid box section, Fig. 1.a); therefore, we can make a step forward by designing tunnel and station sections with low lateral stiffness.

As this proposal might raise relevant construction problems, this paper analyzes a relevant case study: Daikai Station (Kobe, Japan), seriously damaged by the Great Hanshin Earthquake in 1995 [20–23]. This situation is chosen as the world's most relevant example of actual cut-and-cover underground structure having been severely affected (even some sections collapsed) by seismic activity; moreover, as expected, this case has received worldwide attention, and many investigations and studies have been reported. The viability of the proposed solution has been preliminarily validated in an earlier paper

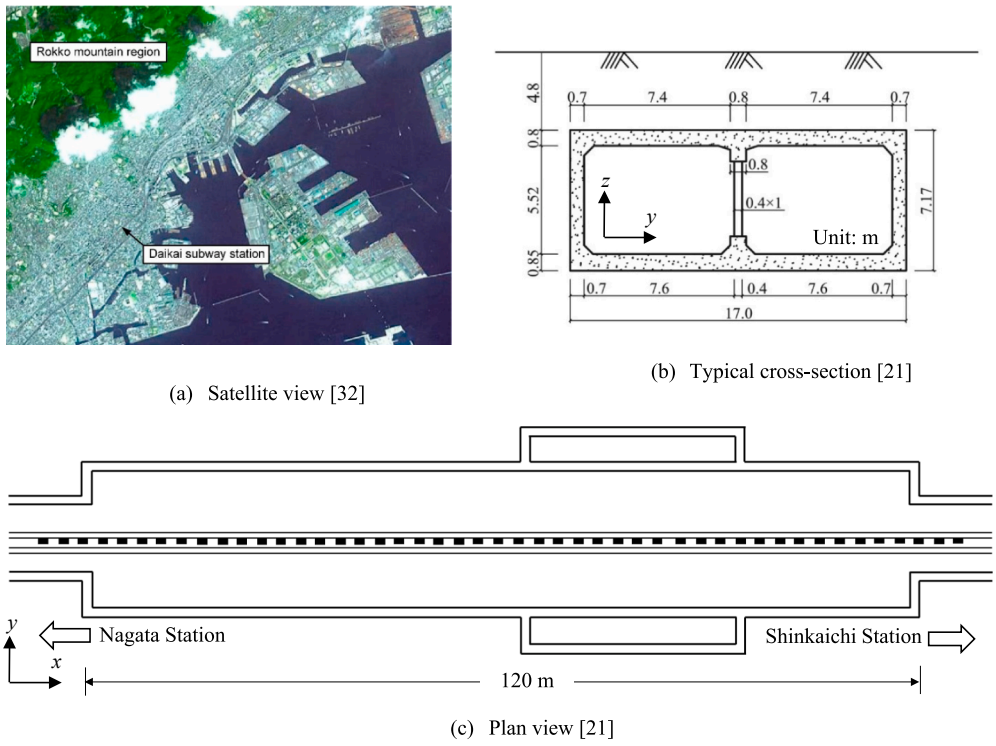

(a) Satellite view [32]

(b) Typical cross-section [21]

(c) Plan view [21]

Fig. 4. Daikai Station.

by the same authors [24]; it presents a supplementary case study on a 2-story 3-bay subway station located in Chengdu (China). It is expected that the correct solution of these two emblematic problems can corroborate the feasibility of the offered alternative solution (Fig. 2.a and Fig. 2.c).

The proposed approach in Fig. 2.a and Fig. 2.c apparently refers to cast-on-site construction; however, it can be utilized for both cast-in-place and precast [6,25–28] structures.

The solutions in Fig. 2.a and Fig. 2.c might look to be unstable structures; however, once the construction is complete, the surrounding soil will provide sufficient protection to prevent excessive lateral displacement (drift). Nevertheless, during construction, temporary bracing might be necessary. On the other hand, large residual drift will be blandly accommodated; therefore, the proposed solution might not be suitable for laterally sloping terrain, mostly near the horizontal ground surface. For further confirmation, Appendix A presents a detailed structural analysis of the Daikai Station (retrofitted with the proposed solution) undergoing asymmetric surface static loading.

3. Daikai station

3.1. Background

The above considerations on the rather high seismic vulnerability of cut-and-cover underground structures are corroborated by a number of observed damages in actual structures; some relevant situations have been reported, as a cut-and-cover railroad tunnel with brick lining destroyed by the 1906 San Francisco earthquake, and five cut-and-cover conduits and culverts with reinforced concrete linings damaged during the 1971 San Fernando earthquake [29]. However, the most important and better described case is the Daikai Station (Kobe, Japan), affected by the Great Hanshin (Kobe) Earthquake (January 17, 1995, $M_w = 6.9$) [20–23,30,31]. The Daikai Station is located in the northwest of Chuo Ward of Kobe, Hyogo, Japan (Fig. 4.a). Fortunately, neither fatalities nor seriously injured people were informed. It took approximately one year before the station was fully restored to normal service.

3.2. Daikai station description

Fig. 4 describes the Daikai Station; Fig. 4.a shows a satellite view, Fig. 4.b displays a typical cross-section, and Fig. 4.c presents a plan view.

The station is rather shallow (the overburden height ranges between 1.9 and 4.8 m). Fig. 4.b shows one of the cross-sections that collapsed during the earthquake; it is a box-type single-story rectangular transverse section (17 m wide and 7.17 m high) with a row of columns at its middle. The column width (x direction) is 1 m, and the clear length between consecutive columns is 2.5 m. The excavation was cut-and-cover; there were no diaphragm walls, albeit a sheet pile wall supported the excavation [31]. Noticeably, all the structural connections (between walls, slabs and columns) were rigid (as in Fig. 1.a and Fig. 4.b). The soil consists of relatively loose silty and clayish sand (Fig. 10.b), with the water table depth ranging between 6 and 8 m; the shear wave velocity of each soil layer ranges between 140 and 500 m/s [20,21,23,33]. As shown in Fig. 4.b, there are no foundation piles.

3.3. Damage of Daikai station during the Kobe earthquake

Fig. 5 [34] describes the observed seismic damage of the Daikai Station; Fig. 5.a shows that a big number of the central columns collapsed, and Fig. 5.b depicts the ensuing affectation of the soil surface (an area about 100 m long, with 2.5 m maximum settlement). Fig. 5.c and Fig. 5.d display images of the most severely damaged columns and the settled soil surface, respectively; Fig. 5.c also contains a sketch of the most collapsed column and its influence on the frame deformation. Fig. 5.c shows that, apparently, the column longitudinal reinforcement buckled due to insufficient hooping.

Other subway facilities in Kobe were also damaged (both in the metro system and the Kobe Rapid Transit Line), although to a lesser extent [21,23,35]. Notably, the adjoining tunnel segments (also cut-and-cover sections, although 9 m wide and 6.36 m high) were less damaged, despite being allegedly weaker; this trend can be understood as a corroboration of the suitability of the strategy proposed in this paper.

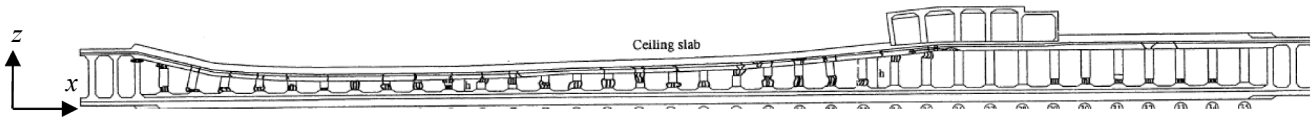

(a) Longitudinal section [21]

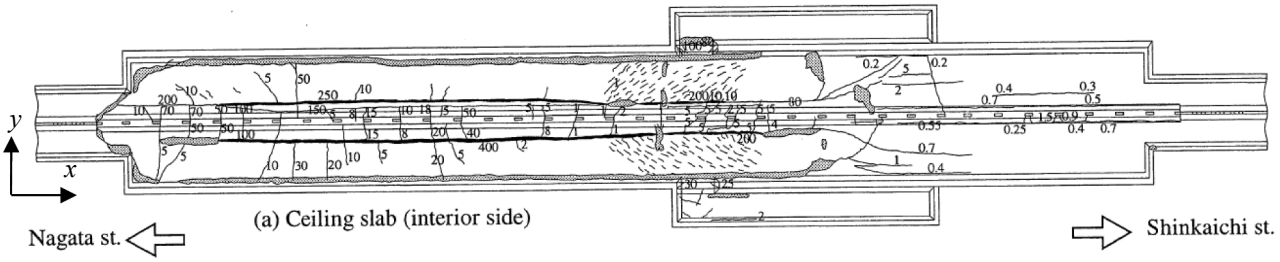

(b) Plan view [21]

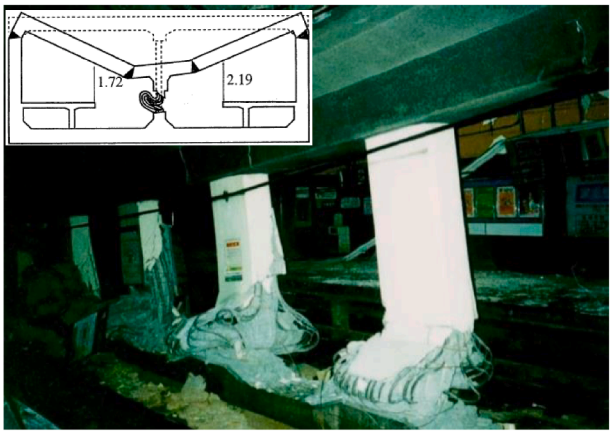

(c) Collapse of center columns [21,34]

(d) Roadway settlement [34]

Fig. 5. Seismic damage of the Daikai Station during the Kobe earthquake.

3.4. Seismic retrofit of the Daikai station

The Daikai Station was retrofitted by removing the overburden and the damaged parts (ceiling slab, central column, and the upper part of the side walls) and designing and rebuilding them according to the seismic standards [31,36]; particular attention was paid to the column transverse reinforcement. The issues that are more relevant to the research in this paper are analyzed later in subsection 5.2. Noticeably, broadly speaking, the final appearance of the station (after the retrofit) is similar to the initial one.

3.5. Reported research on the Daikai station damage

A number of papers discussing on this collapse have been published [32–34,37–50]; in fact, this case is still being investigated. These researches highlight that the shear reinforcement of the central column was insufficient, and that the vertical component of the seismic action played a relevant role.

Summing up, the major conclusions arising from this collapse are: (i) the cut-and-cover subway stations are, apparently, one of the most vulnerable underground structures, (ii) the lateral static redundancy (hyperstaticity) of the Daikai Station (rigid connections between its structural members) played a highly negative role, (iii) the effect of the vertical seismic action was highly significant, increasing the axial compressive ratio of the central columns and thus deteriorating their ductility, (iv) the transverse reinforcement in the critical sections of the columns (top and bottom ends) is very necessary to provide shear strength and ductility, and to prevent buckling of the compressed longitudinal reinforcement, and (v) the soil-structure interaction is of paramount importance. Remarkably, the actual station retrofit, and the vast majority of the earlier reported researches consider issues i, iii, iv and v, but not ii.

3.6. Reported research on alternative solutions for the Daikai station

As discussed in section 1, the main objective of this research is to propose alternative solutions for cut-and-cover stations and tunnels (valid for retrofit and new construction). In this direction, some papers proposing non-conventional approaches (for the Daikai Station and other underground structures) have been published; they focus on the central columns, which are considered to be the key components. The reported solutions can be broadly classified into seismic isolation and seismic reduction technologies; both sets of approaches are discussed in the next paragraph.

Most of the studies suggest isolating structurally (seismically) such elements by using different technologies that provide lateral flexibility: rubber bearings coated by curved steel plates [51], LRB (Lead-Rubber Bearing) [52], RFPS (Roller Friction Pendulum System) [53], sliding isolation bearings (using steel rolling balls) [54,55], LNB (Laminated Rubber Bearing) [56], and central rocking columns with friction dampers [57]. Also, [58] considered lead-core rubber bearings (LRBs) to isolate the columns of a three-story subway station in Shanghai.

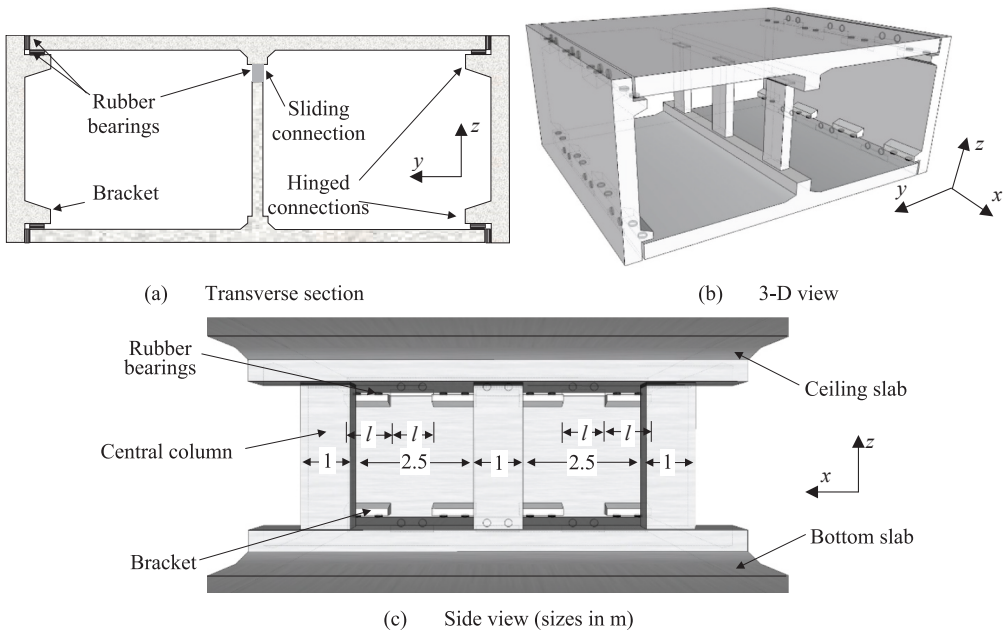

Fig. 6. Proposed hinged-sliding solution (S2) for the Daikai Station.

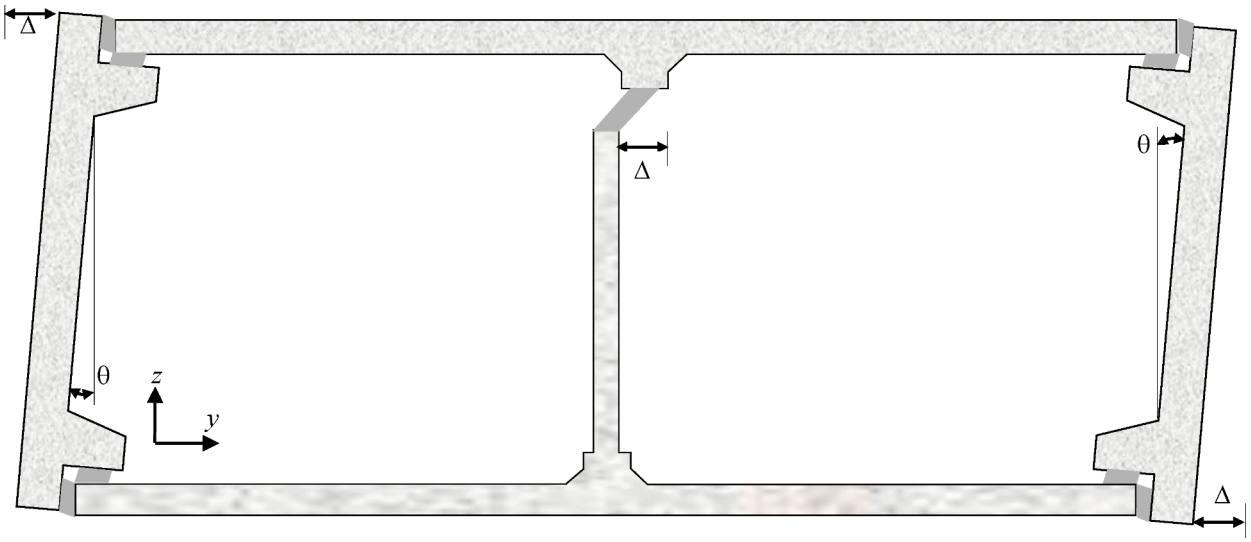

Fig. 7. Racking behavior of the proposed low lateral stiffness structural solution S2 for the Daikai Station.

Regarding energy dissipators (seismic reduction), [12] considers a shear panel damper intended to absorb energy, [59] proposes lead-filled steel tube dampers, and [50] presents a novel laterally deformable column ("segmental cored column"). Finally, going back to the Daikai Station, [60] proposes inserting shock absorbing devices between the sidewalls and the ceiling slab, in order to reduce the lateral forces on the central columns.

4. Proposed hinged-sliding solution for the Daikai station

4.1. General description of the proposed solution

In the alternative solutions mentioned in subsection 3.6, the external box is still rigid (moment-resisting frame). Conversely, this paper presents a more radical option for the Daikai Station, with not only a central column rather seismically isolated from the box, but also hinged connections between walls and slabs; the core feature of this solution is its low transverse lateral stiffness, so as not to be affected by the soil shear strains generated by the seismic shear waves. Fig. 6 displays sketches of the intended approach (S2, subsection 4.1); Fig. 6.a presents a front view (transverse section), Fig. 6.b contains a 3-D representation, and Fig. 6.c shows an internal lateral view (longitudinal section). The coordinates (x, y, z) in Fig. 6 are maintained along this paper.

Fig. 6.a shows that the aforementioned external box is composed of four fully hinged members: two side walls and the top (ceiling) and bottom slabs; the connections between them consist of horizontal and vertical rubber pads with embedded steel shims (to provide high axial stiffness yet keeping high transverse flexibility). The walls have two short cantilevers (brackets or corbels) near their top and bottom ends, to prevent downward and upward displacement of the ceiling and floor (bottom) slabs, respectively. The column is rigidly connected to the floor slab, but its connection to the roof is rather sliding; the release of the relative horizontal displacement between both members is granted by a pretty slender rubber pad. It should be noted that such a structural

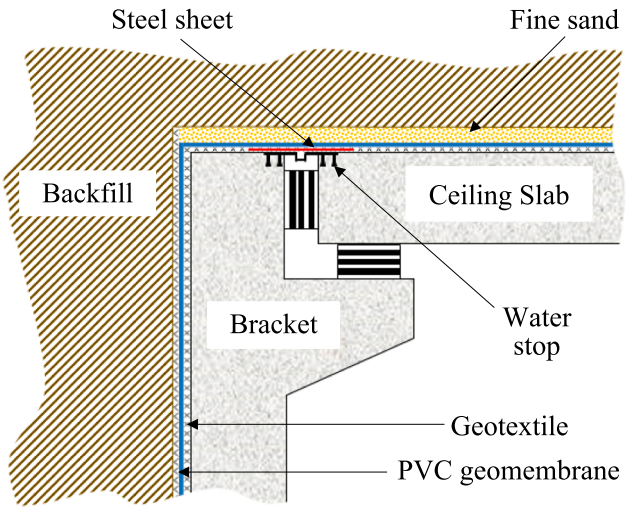

Fig. 8. Watertight system of the proposed hinged-sliding solution S2.

discontinuity can be introduced at any column section, not just at the top. Fig. 6.b and Fig. 6.c show that the aforementioned wall brackets are not continuous along the tunnel length, but are regularly interrupted by interposing equal-length (l) segments with and without brackets. The main objective of this arrangement is to facilitate the access of the rubber pads for maintenance purposes; in order to do this, the segments with/without brackets have only horizontal/vertical pads, respectively. Fig. 6.c also shows that the column width is 1 m, and the clear separation between consecutive columns is 2.5 m (subsection 3.2).

The proposed hinged and sliding connections can be built using different technologies; in this preliminary study, the use of rubber bearings is proposed. These elements are perfectly able to resist vibrations generated by railway traffic; even some devices (HDRB, High-Damping Rubber Bearings) are particularly well suited to absorb (damp out) such vibrations.

In the rest of the paper, three solutions are compared: classical rigid design **S0** (Fig. 4.b and Fig. 16.b), low lateral stiffness **S2** (Fig. 6, Fig. 7 and Fig. 16.d), and an intermediate situation **S1** that combines rigid connections between walls and slabs with a sliding connection between the central column and the top slab (Fig. 16.c). This last case has been incorporated since it has been proposed by several researchers [51–57]. As discussed later (subsection 5.5), the characteristics of the main structural elements (walls, slabs and column) are similar in solutions S0,

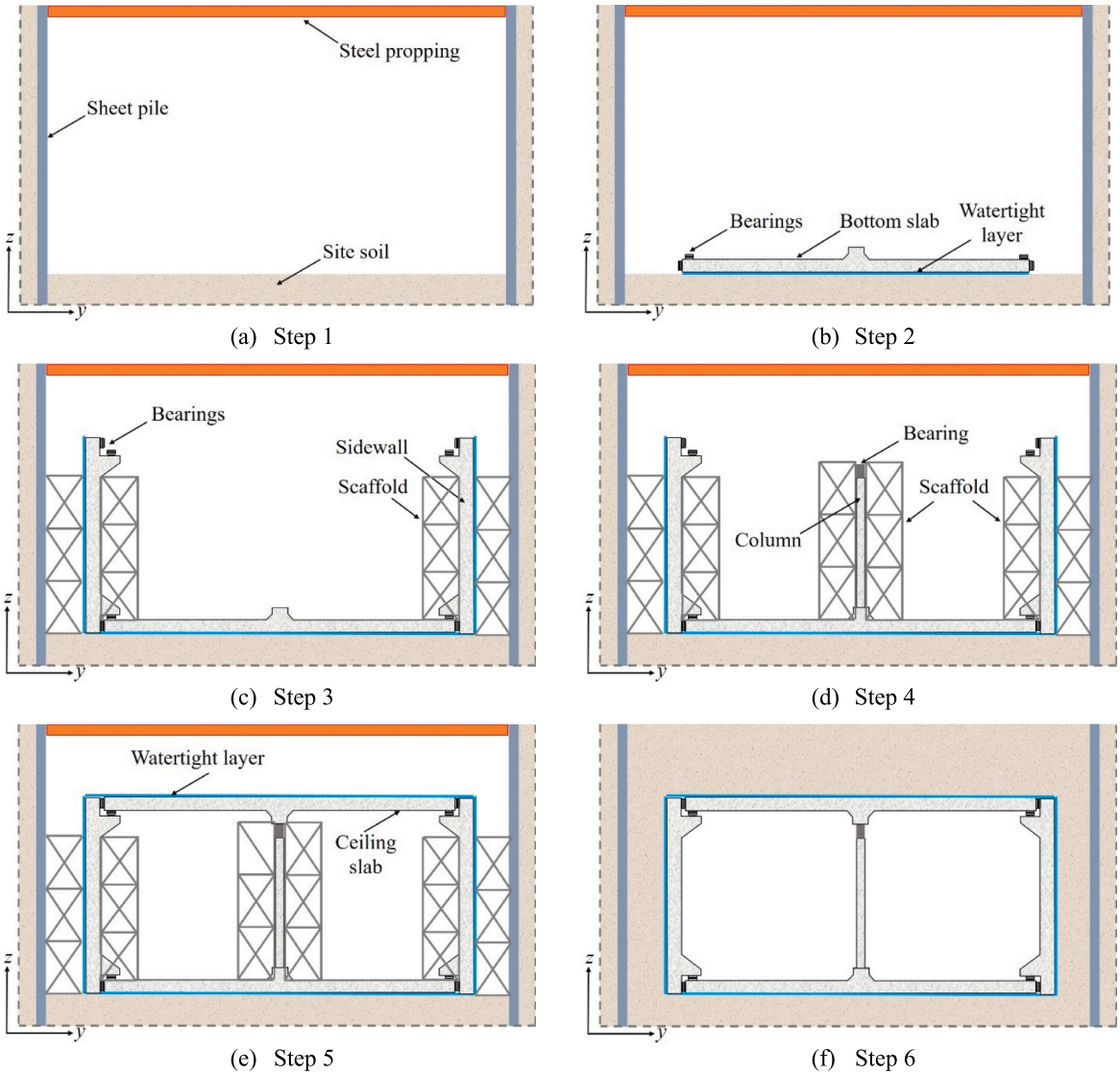

Fig. 9. Major steps of the construction process of the proposed solution S2.

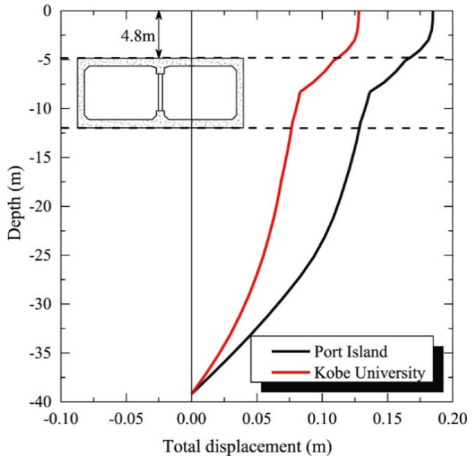

(a) Computed displacement

Depth (m)	Density (t/m^3)	Shear wave velocity (m/s)	Poisson ratio
0 - 1	1.9	140	0.333
1- 5.1	1.9	140	0.488
5.1 - 8.3	1.9	170	0.493
8.3 - 11.4	1.9	190	0.494
11.4 - 17.2	1.9	240	0.490
17.2 - 39.2	2	330	0.487
> 39.2	2.1	500	0.470

(b) Soil profile at Daikai Station

Fig. 10. Approximate free-field racking deformation for the Kobe earthquake closest to the Daikai Station [40].

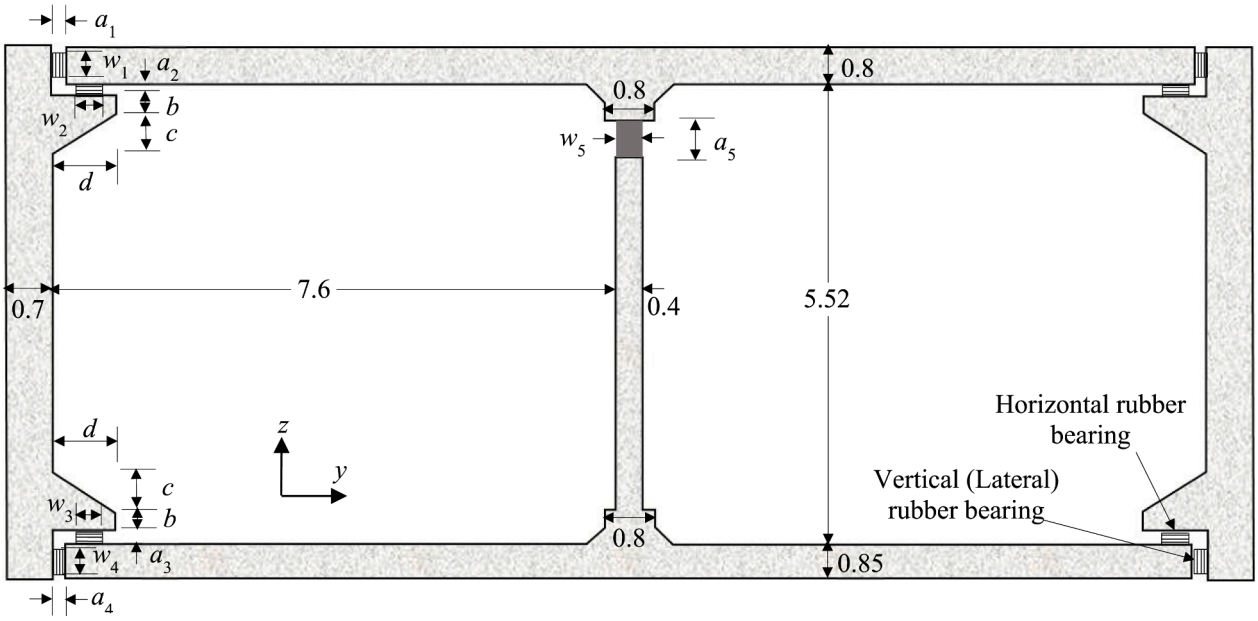

Fig. 11. Major sectional dimensions of the proposed alternative solution S2 for the Daikai Station. Sizes in m.

S1 and S2. Comparison with the general structures depicted in Fig. 2 shows that, broadly speaking, solution in Fig. 1.a would correspond to S0, while Fig. 2.a and Fig. 2.c can be considered as S2.

4.2. Racking behavior of the proposed solution S2

Fig. 7 displays, analogously to Fig. 2.b, a representation of the racking deformation of the proposed alternative tunnel solution S2 (Fig. 6.a). In Fig. 7, θ is the rotation angle of the wall with respect to the slab, and Δ is the relative horizontal (racking) displacement between the column and the ceiling slab; Fig. 7 shows that it is equal to the global racking displacement.

The rubber bearings are designed (subsection 5.6) to absorb the relative motions (bending rotation and shear displacements) between the members they connect; this includes the local elongations (tensile stresses) (subsection 8.5).

4.3. Watertight system of the proposed solution S2

The rotation capacity of the wall-slab connections together with the required gaps (a_1 and a_2, Fig. 11), makes that, in the proposed alternative solution S2, water tightness is more difficult than in the original rigid box section (Fig. 4.b); therefore, this study must address this issue.

Several waterproofing systems have been developed for tunneling, and they are nowadays technically mature; a comprehensive description of such procedures is included in [61]. More recent works describe systems for different contexts: [25] in prefabricated elements in cut and cover tunnels, [62] and [63] in immersed tunnels, and [64] in segmental tunnels. Here, a conventional watertight system based on impervious flexible membranes (made of high-density polyethylene) and joints/water stops [61] is presented in Fig. 8.

Fig. 8 shows that the proposed system consists, from the outside to the inside, of the following layers: protective fine sand (only on the horizontal surfaces), a watertight PVC geomembrane, and a geotextile.

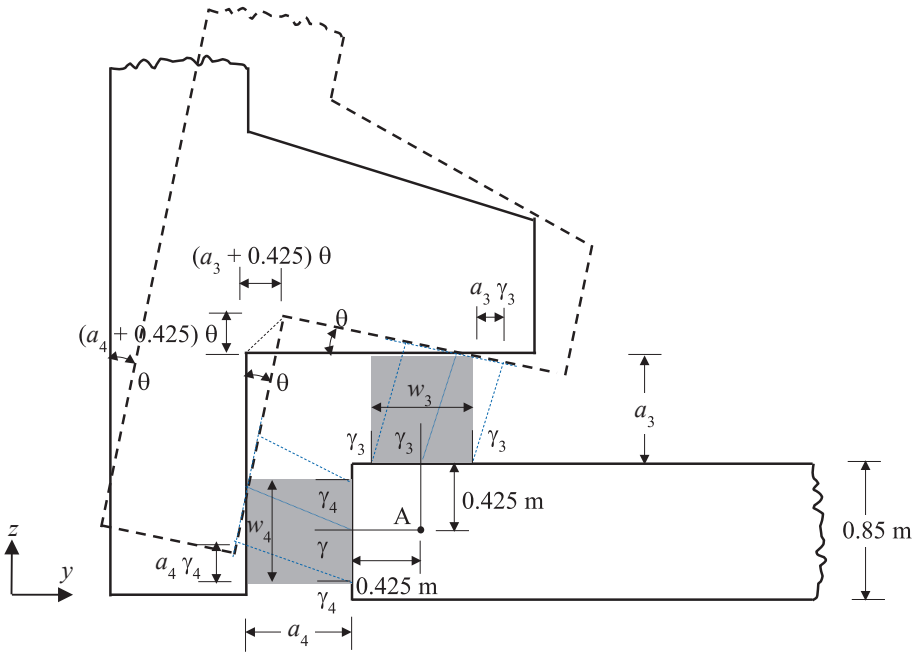

Fig. 12. Assumed kinematic deformation of the hinged connection between the left wall and the lower slab during the racking deformation (solution S2).

Moreover, in the upper horizontal gap (a_1, Fig. 11), two additional elements are placed: a steel plate, and a rubber water-stop expansion joint; the main objective of the steel plate is to provide mechanical strength while allowing relative displacement between the side wall and the ceiling slab. The purpose of the fine sand layer is to protect the PVC geomembrane during compaction and other operations.

Globally speaking, it should be noted that for cut and cover tunnels, the water pressure acting on the lining is low, and, therefore, the requirements in terms of waterproofing are quite easy to meet.

4.4. Construction process of the proposed solution S2

As discussed previously, the proposed solution S2 is intended for both new construction and retrofit. This section describes the process for new construction; the strategy for retrofit would be rather similar, basically requiring the near total removal of existing elements.

The construction of the alternative proposed solution S2 is not as different from the conventional one. The major steps are outlined in Fig. 9 and discussed below:

1. Installation of two sheet pile walls at both sides of the station, water table lowering, soil excavation between the sheet piles, and placement of a temporary horizontal top steel propping system (Fig. 9.a). This step has different alternatives, depending on the soil properties and the water table level: diaphragm walls are also possible, use of anchors, and, when there is available space, soil excavation with lateral slopes is feasible as well. Obviously, the design of the dewatering must be adapted to the local geometry of the performed excavation.
2. Watertight system in the excavation bottom, floor slab (molds, reinforcement and concrete pouring), and lateral and horizontal rubber bearings in that slab (Fig. 9.b); the bearings (either horizontal or vertical) are fixed to the structural members they connect. Typically, water-tightness is achieved by means of geomembranes or geocomposites that surround the whole structural section (subsection 4.3).
3. Side walls (molds, reinforcement and concrete pouring), top lateral and horizontal rubber bearings, and lateral watertight system (Fig. 9.c).
4. Central columns (molds, reinforcement and concrete pouring) and top rubber bearing. Obviously, this step and the previous one are totally interchangeable (Fig. 9.d).
5. Ceiling slab (molds, reinforcement and concrete pouring), and top watertight system (Fig. 9.e).
6. Soil filling and compaction, and removal of the propping system (Fig. 9.f). Backfilling operations should be carried out keeping the symmetry of the geometry as much as possible, to avoid unbalanced earth pressures on the lateral tunnel sidewalls.

These operations can be easily modified to include other common elements, such as diaphragm walls or foundation piles. In addition to that, prefabrication of most of the elements of the structural section [25,26,65] is also possible, and in that case longitudinal gasketed joints between elements should be provided to guarantee waterproofing [25]. Such combination would make it possible to merge the advantages of the proposed technology and those of prefabrication.

The influence of the lateral walls used to protect the excavation (e.g. sheet piles, Fig. 9.a) on the tunnel seismic response might prove important as the gap between them and the tunnel sidewalls may affect their coupled response. For the Daikai Station, [3] indicates that this narrow clearance resulted in a poor backfill compaction, and therefore passive pressure did not develop. In general, the flexibility of the lateral walls should be high to avoid any additional constraint to the soil motion, thus keeping the tunnel section flexible.

5. Design and verification of the proposed solution S2 by simplified hand structural analysis

5.1. General description of the simplified analysis for solution S2

This section presents an abridged static equivalent analysis of the seismic performance of the Daikai Station under the Great Hanshin (Kobe) earthquake. As the objective of this study is to corroborate the suitability of the proposed solution S2, the structure is assumed to be equipped with the protective rubber elements described in Fig. 6 and Fig. 7.

In subsection 5.2 the seismic free-field demand is approximately estimated, in subsection 5.3 a rigid-body model of the racking behavior

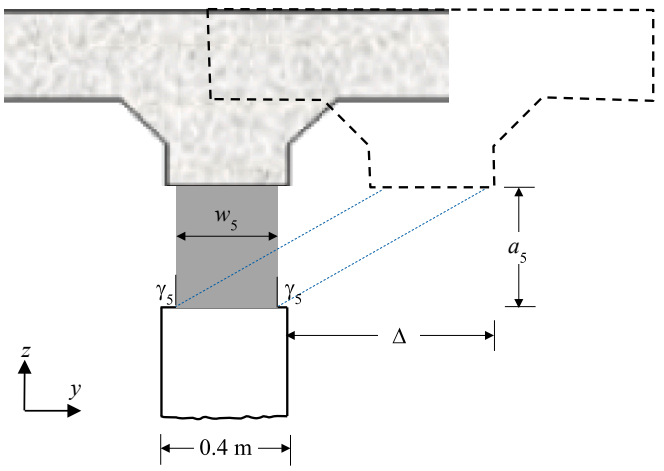

Fig. 13. Assumed kinematic deformation of the ceiling slab-column sliding connection during the racking deformation (solution S2).

of the station is described, and in subsection 5.4 the internal forces in the main structural members of the station (walls, slabs and column) are determined by a conventional linear elastic analysis. Then, in subsections 5.5 and 5.6, the sizes of such members and of the rubber bearings are approximately determined, respectively. Finally, in subsection 5.7, the racking displacement in the station is obtained.

Noticeably, although the analysis described in this section might look as over-simplified, all the assumptions are firmly grounded in logical considerations, and the results are reasonably accurate and totally reliable. More precisely, given the high uncertainty of all the issues involved (soil, structure and seismicity), the accuracy and reliability of this analysis are comparable to those of the allegedly more exact calculations described in sections 6–8.

5.2. Approximate estimation of the demand free-field racking displacement

In order to provide input data for the aforementioned simplified soil-structure interaction analysis, Fig. 10.a [40] displays the computed free-field soil response to the accelerograms that were recorded closest to the Daikai Station (i.e. Port Island and Kobe University); Fig. 10.b exhibits the main parameters of the soil profile of Daikai Station.

The two plots in Fig. 10.a represent the soil profile deformation at the moment when the relative displacement between the ceiling and bottom slabs is maximum; such free-field displacements are 38.79 mm and 35.57 mm for the Port Island and Kobe University records, respectively. As the first value is more demanding, is adopted in this study.

5.3. Rigid-body model of the racking behavior of the proposed solution S2

Fig. 11 displays a detailed transverse view of the proposed solution S2. Note that the brackets do not affect the station operation. Regarding the other elements, their shapes are equal to those of the actual station; consequently, they do not cause any modification either. This is further discussed in subsection 5.4.

In Fig. 11, a_1, a_2, a_3, a_4 and a_5, on one side, and w_1, w_2, w_3, w_4 and w_5, on the other side, are the rubber bearings height (thickness) and width, respectively. Finally, b, c and d are the dimensions of the brackets (corbels, Fig. 6).

In Fig. 7, only the rubber bearings experience some deformation, while the concrete elements are assumed to remain undeformed. On the other hand, given that the deformation due to the seismic vertical waves is significantly smaller than that of horizontal (lateral) ones, it is assumed that the top and bottom slabs almost do not rotate (with respect to the longitudinal axis x). These suppositions provide the following kinematic relationship between the wall rotation angle, θ, and the transverse racking displacement, Δ:

$$\Delta = 7.17\,\theta\,\text{m} \tag{1}$$

In equation (1), 7.17 m is the total height of the side wall (Fig. 4.b).

In order to provide a deeper insight into the rubber bearings deformation, Fig. 12 displays a zoom view of the bottom left corner rotation of the frame in Fig. 7 and Fig. 11. Note that the pads undergo both shear and bending deformation. In Fig. 12, γ_3 and γ_4 are the shear strains in the horizontal and vertical (lateral) rubber bearings, respectively; remarkably, γ_3 and γ_4 are not equal to the rubber strain, due to the presence of steel layers. Noticeably, the vertical bearing is centered with respect to the mid line of the bottom slab; for simplicity, as shown in Fig. 12, the same type of position is maintained for the horizontal bearing.

The situation described in Fig. 12 corresponds to rigid-body motion of the wall and the slab; as considered in Fig. 7, the rubber bearings concentrate all the deformation, since they are significantly more flexible than the main concrete bodies. Given the rather high axial stiffness of the rubber bearings (due to the transverse confinement effect of the aforementioned steel plates), their average axial strain has been assumed to be zero; this simplification is acceptable, as the objective of this paper is not to provide a highly accurate design, but to demonstrate the feasibility of the proposed alternative construction solution S2. As long as $a_3 = a_4$, the rigid body motion of the left side wall is a pure rotation, and its center is located at the intersection between the corresponding horizontal and vertical lines (point A in Fig. 12).

The motion depicted by Fig. 12 corresponds to a small rotation angle θ; therefore, the angles (in radians) are assumed to be equal to their tangent and sine, and their cosine equal to 1. This supposition provides the following kinematic relationship between the wall rotation angle and the shear strain in the bearings:

$$(a_3 + 0.425)\,\theta = a_3\,\gamma_3 \qquad (a_4 + 0.425)\,\theta = a_4\,\gamma_4 \tag{2}$$

In equations (2), a_3 and a_4 must be expressed in m. Equations similar to (2) can be formulated for the top corner bearings by replacing subscripts 3 and 4 with 1 and 2, respectively (Fig. 11).

Fig. 13 displays, similarly to Fig. 12, a zoom view of the lateral sliding between the central column and the ceiling slab (Fig. 7). In Fig. 13, γ_5 is the shear strain in the column bearing.

Fig. 13 provides the following kinematic relationship between the racking displacement (Fig. 7) and the shear strain in the column bearing:

$$\Delta = a_5\,\gamma_5 \tag{3}$$

This subsection shows that the lateral stiffness of the station is not actually zero, but depends on that of the rubber bearings. The obtained value is described in subsection 6.2.6.

5.4. Internal forces laws in the main structural members of solution S2

The design transverse pushing forces for the Daikai Station with the proposed hinged-sliding solution S2 (Fig. 6 and Fig. 16.d) are obtained from the values proposed in [31] for the actual retrofit (in the most critical transverse section corresponding to 4.8 m overburden, Fig. 4.b). The following loading cases were considered in such retrofit: 1 (dead load + live load), 2 (dead load), 3 (racking effect), 4 (downward vertical inertia) and 5 (upward vertical inertia). The water buoyancy forces are included in case 1, and correspond to the water table being 10.545 m above the station bottom level. The most demanding combination for the actual retrofit included cases 2, 3 and 4 (or 5); conversely, in the proposed hinged-sliding solution S2, it is assumed that the frame structure would not be influenced by racking effects (case 3) because of its low lateral stiffness. Therefore, the most unfavorable situation is **1.2 × case 2 + 1.3 × case 4** (these safety factors have been obtained from the Chinese regulations [66]). The corresponding demand forces are

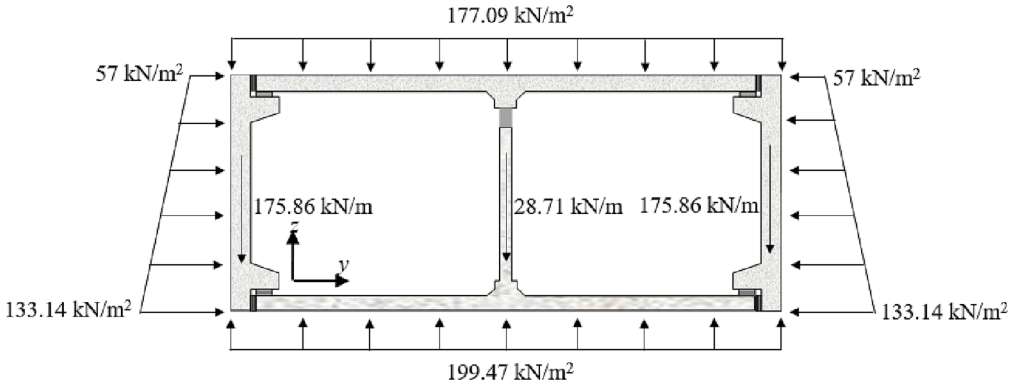

Fig. 14. Approximate design forces for the proposed low lateral stiffness solution S2 for the Daikai Station (1.2 × case 2 + 1.3 × case 4).

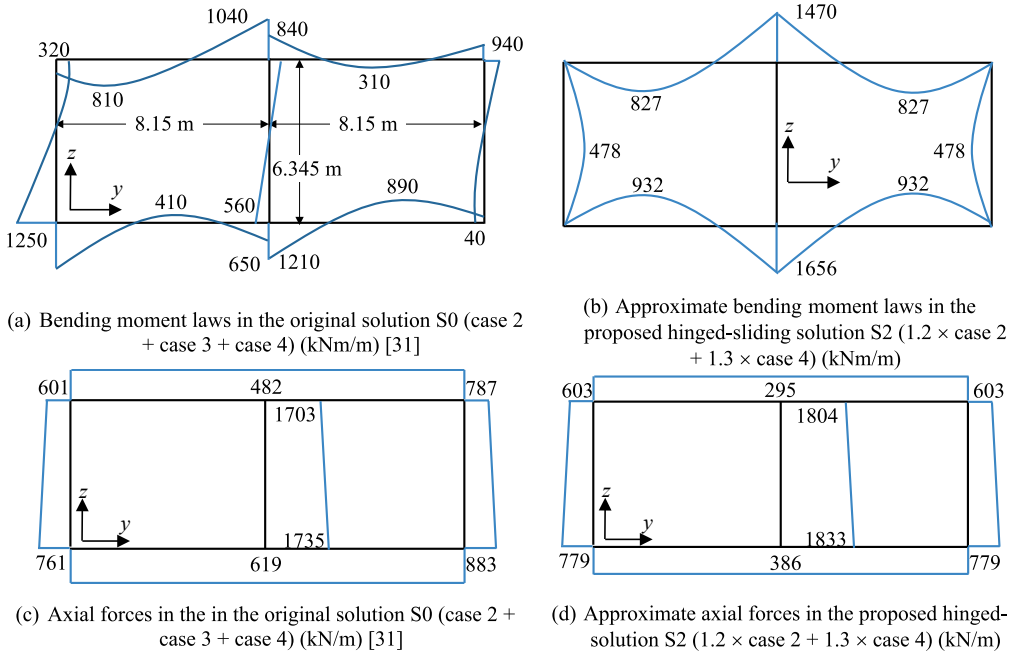

(a) Bending moment laws in the original solution S0 (case 2 + case 3 + case 4) (kNm/m) [31]

(b) Approximate bending moment laws in the proposed hinged-sliding solution S2 (1.2 × case 2 + 1.3 × case 4) (kNm/m)

(c) Axial forces in the in the original solution S0 (case 2 + case 3 + case 4) (kN/m) [31]

(d) Approximate axial forces in the proposed hinged-solution S2 (1.2 × case 2 + 1.3 × case 4) (kN/m)

Fig. 15. Approximate internal forces in the Daikai Station for the most demanding situations for solutions S0 (Fig. 16.b) and S2 (Fig. 16.d).

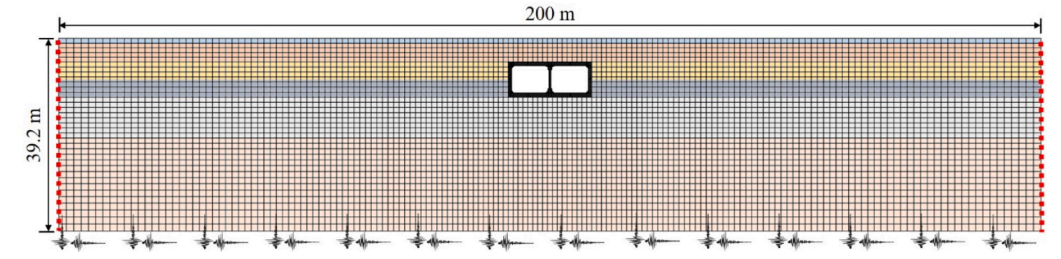

(a) Soil mesh

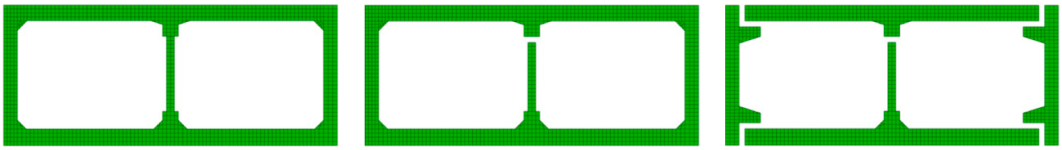

(b) Station mesh. Solution S0 (c) Station mesh. Solution S1 (d) Station mesh. Solution S2

Fig. 16. Finite element models of the Daikai Station (solutions S0, S1 and S2) and the surrounding soil.

Table 1
Approximate demand parameters for the rubber bearings (S2).

Bearing	Axial force (kN)	Shear displacement $a_i\,\gamma_i$ (mm)	Rotation angle θ (mrad)
Top corner vertical (lateral) bearing	295*	$(a_1 + 0.425)\,\theta$	10.82
Top corner horizontal bearing	603*	$(a_2 + 0.425)\,\theta$	10.82
Bottom corner vertical (lateral) bearing	386*	$(a_3 + 0.425)\,\theta$	10.82
Bottom corner horizontal bearing	779*	$(a_4 + 0.425)\,\theta$	10.82
Top of central column	6314**	77.58	–

*1 m length; **3.5 m length; a_1, a_2, a_3, a_4 in m.

displayed in Fig. 14.

In Fig. 14, the self-weight is obtained assuming a concrete unit weight 25 kN/m^3; in this operation, the discontinuous central columns (Fig. 5, Fig. 6.b) have been replaced by an equivalent fictitious continuous wall. The beneficial effect of the bottom slab self-weight has been disregarded; in fact, the most demanding combination for that element is **1.2 × case 2 + 1.3 × case 4**.

The internal forces of the structure represented in Fig. 14 are determined by linear elastic global structural analyses per unit length (1 m) of the station. Fig. 15 displays relevant internal forces diagrams of the original (S0) and alternative solutions (S2); Fig. 15.a and Fig. 15.c correspond to the actual retrofit (solution S0) [31], and Fig. 15.b and Fig. 15.d stand for the hinged-sliding structure (solution S2, Fig. 14). Fig. 15.b and Fig. 15.d present the bending moments and axial forces, respectively; regarding the shear forces, are not included as being easily obtained from the axial ones (by equilibrium conditions of proper portions of the structure). In these last Figures, the black lines correspond to the axes of the structural members (walls, slabs and column); Fig. 15.a shows the span-lengths of slabs, and the heights of walls and column. The moments are obtained for such lengths; in other words, they are related to the part of the loads that is comprised between the axes of the structural elements. Conversely, the axial forces correspond to the total load. Noticeably, in Fig. 15 the load combinations for solutions S0 and S2 have been used; this make sense, as the most demanding situations for each case have been selected.

Comparison between the bending moments and axial forces of the conventional (S0, Fig. 15.a and Fig. 15.c) and alternative (S2, Fig. 15.b and Fig. 15.d) solutions shows that they are rather similar. However, such internal forces in solutions S0 and S2 cannot be compared directly, as the loads are different (because of the assumed hypotheses and the safety factors); for instance, the difference between the maximum positive and negative values in each slab in Fig. 15.a and Fig. 15.b shows that in solution S2 the loads on that slabs are higher. Therefore, no big changes in the walls and slabs thickness and reinforcement amounts are expected; as previously announced, this circumstance endorses the proposed solution S2 (Fig. 11). Regarding Fig. 15.d, the axial compressive forces in the side walls and in the central column cannot be highly different from those of the traditional solution S0, as their sum is constant (equal to the supported load). Finally, Fig. 15.b and Fig. 15.d show that the risk of damage to the central columns is significantly reduced in solution S2, as the moment is dramatically reduced while the axial forces are similar.

5.5. Design of the main structural members for the proposed solution S2

As discussed in subsection 5.4, the demanding internal forces in the actual (S0) and hinged-sliding solutions (S2) are not very different; therefore, equal sizes (Fig. 4.b) and similar reinforcements are considered for walls, column and slabs. Regarding the corbels for solution S2 (brackets, Fig. 11), the following transverse (y and z) and longitudinal (x) dimensions are selected [67]:

$$b = 300\ \text{mm} \quad c = 600\ \text{mm} \quad d = 600\ \text{mm} \quad l = 1000\ \text{mm} \tag{4}$$

The values in equation (4) are chosen to be sufficient for structural purposes, yet not affecting the station function.

5.6. Design of the rubber bearings for the proposed solution S2

The bearings are conventional rubber devices that are internally confined by steel plates to provide fairly high axial stiffness (taking advantage of the elevated rubber Poisson ratio) while maintaining important lateral flexibility (necessary to accommodate the required shear strain, Fig. 12 and Fig. 13). In the situations analyzed in this paper, the rubber bearings should be flexible enough to adapt the required (bending) relative rotation between their ends (Fig. 12). Therefore, the most relevant demand parameters for the rubber bearings are: axial compressive force, shear strain, and bending rotation angle. Table 1 displays the values of such parameters; the axial force is obtained from Fig. 15.d, the shear strain is given by equations (2) and (3) (for the walls and column bearings, respectively), and the rotation (θ) is specified later in subsection 5.7. For the wall bearings, the displayed forces correspond to 1 m of tunnel, while for the column bearing it corresponds to 3.5 m (the length spanned by a single column, Fig. 6.b). The rubber bearings are designed to resist their combined demands.

A design of the bearings that fulfills the requirements in Table 1 is proposed. The bearings between slabs and walls (Fig. 12) are circular, while the column bearing is rectangular, to take profit of all the available space in the column top. Table 2 displays the selected geometrical and mechanical parameters.

Comparison between Table 2 and Table 1 shows that the bearing capacities exceed their demands in all the cases. More precisely, equation (4) and Fig. 6.b show that there are two wall-slab bearings per meter length; consequently, the demanding axial force in Table 1 must be split between them.

5.7. Approximate determination of the racking displacement in the station

The demanding racking displacements (in the traditional solution S0 and the proposed hinged-sliding solutions S1 and S2) are estimated by an abridged soil-structure interaction analysis [8,61]. The study [14] considers the influence of the flexibility ratio (F) defined as the quotient between the soil shear stiffness and the station racking stiffness; as

Table 2
Selected characteristics and capacities of the rubber bearings (S2).

Bearing	Diameter or width w_i (mm)	Bearing thickness a_i (mm)	Maximum axial force (kN)	Maximum shear displacement $a_i\,\gamma_i$ (mm)	Maximum rotation angle θ (mrad)
Wall-slab connections (1–4)	300 (Diameter; w_1, w_2, w_3, w_4)	130 (a_1, a_2, a_3, a_4)	900	± 50 ($a_1\gamma_1$, $a_2\gamma_2$, $a_3\gamma_3$, $a_4\gamma_4$)	($a_1\gamma_1$, $a_2\gamma_2$, $a_3\gamma_3$, $a_4\gamma_4$)
Top of central column (5)	1000 × 400 (w_5)	175 (a_5)	6500	80 ($\Delta = a_5\,\gamma_5$)	35

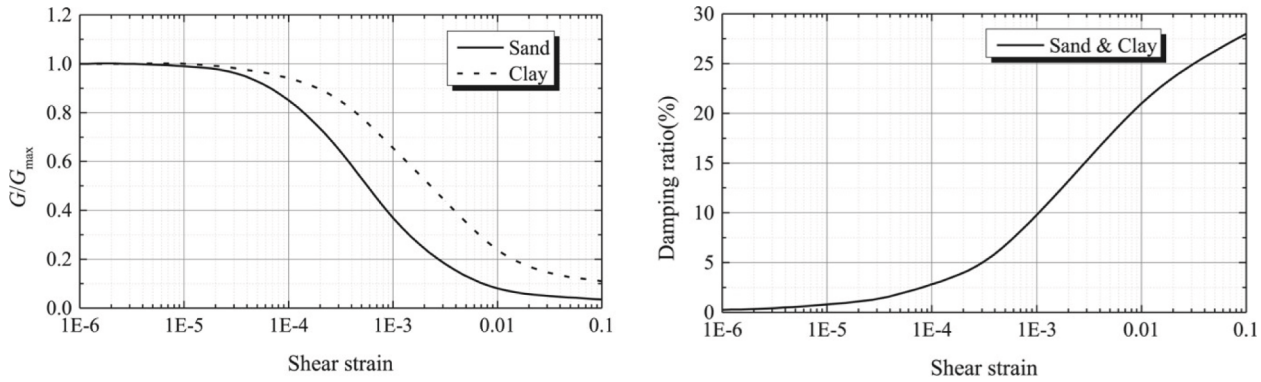

(a) G / G_{max} vs. shear strain curves of the soil (b) Damping ratio vs. shear strain curves of the soil

Fig. 17. Constitutive curves of the soil [39].

expected, if $F < 1$, the tunnel racking distortion is smaller than the soil free-field deformation, and if F greater than 1, the opposite situation occurs.

The station racking stiffnesses for solutions S0, S1 and S2 are determined in subsection 6.2.6. Regarding soil, its stiffness is calculated with the method by Wang [14]; the obtained value is 41.08 kN/mm (per unit length). Then, the flexibility ratios F are determined as:

$$F_0 = \frac{41.08}{76.6} = 0.536 \qquad F_1 = \frac{41.08}{63} = 0.652 \qquad F_2 = \frac{41.08}{24.6} = 1.67 \tag{5}$$

According to [69], the racking coefficient R (ratio between the racking and free-field displacements) depends on the sliding condition between the structure and the adjoining soil: by assuming free sliding the expression is $R = \frac{4\,(1-\nu)\,F}{3-4\,\nu+F}$, and for prevented sliding it becomes $R = \frac{4\,(1-\nu)\,F}{2.5-3\,\nu+F}$. In these expressions, ν is the soil Poisson's ratio; according to Fig. 10, $\nu = 0.49$ is selected. For that value of the soil Poisson's ratio both expressions of R provide almost the same value:

$$R_0 = \frac{4\,(1-0.49)\,0.536}{3-4\times0.49+0.536} = 0.694 \quad R_1 = \frac{4\,(1-0.49)\,0.652}{3-4\times0.49+0.652} = 0.786 \quad R_2 = \frac{4\,(1-0.49)\,1.67}{3-4\times0.49+1.67} = 1.257 \tag{6}$$

Subsection 5.2 states that the maximum free-field displacement corresponds to the Port Island record, and is equal to $\Delta_{FF} = 38.79$ mm. Then, the racking displacements for solutions S0, S1 and S2 are given by $\Delta = \Delta_{FF}\,R$:

$$\Delta_0 = 38.79 \times 0.694 = 26.92\,\text{mm} \quad \Delta_1 = 38.79 \times 0.786 = 30.49\,\text{mm} \quad \Delta_2 = 38.79 \times 1.257 = 48.76\,\text{mm} \tag{7}$$

According to equation (1), the maximum rotation angles for solutions S0, S1 and S2 are equal to

$$\theta_0 = 26.92/7170 = 3.76\ \text{mrad} \qquad \theta_1 = 30.49/7170 = 4.25\ \text{mrad} \qquad \theta_2 = 48.76/7170 = 6.80\ \text{mrad} \tag{8}$$

These values are required for the structural design of the tunnel and the rubber bearings; will be further compared with the time-history results in subsection 8.2.

6. Verification of the proposed solution S2 by nonlinear time-history analysis

6.1. General considerations

Nonlinear dynamic analyses are conducted to further verify the seismic performance improvement of the Daikai Station featured with low lateral stiffness; more precisely, the three solutions **S0** (Fig. 16.b), **S1** (Fig. 16.c) and **S2** (Fig. 16.d) are compared.

The structural modelling of the station and the surrounding soil is described in subsection 6.2, and section 7 depicts the selected seismic input signals. The analyses are performed under the combined actuation of the horizontal (transverse) and vertical input accelerograms.

6.2. Finite element model for time-history analyses

6.2.1. Modeling of the soil-structure system

A finite element model of the soil-structure system is implemented in ABAQUS [70]; the obtained mesh is displayed in Fig. 16.

Fig. 16.a shows that the soil is discretized with 5656 4-node quadrilateral elements; regarding the station, 1388, 1384, and 1480 elements are utilized for solutions S0, S1 and S2, respectively. In both the soil and the station, 2-D plane strain behavior is assumed. To simulate the seismic wave propagation with sufficient precision, the size of the soil elements must be smaller than 1 / 6 of the minimum wave length λ [71]. By considering a cutoff frequency $f = 25$ Hz, Fig. 10.b shows that $\lambda = v_s / f = 140 / 25 = 5.6$ m for the top layer (just 1 m deep), and $\lambda = v_s / f = 500 / 25 = 20$ m for the bottom layer; therefore, 1 m is an adequate value. Moreover, to further increase the calculation efficiency, the soil areas near the structure are more finely meshed compared to the far-field zones (1 m instead of 1.5 m). Fig. 16.a also shows that the soil is discretized into the six layers described in Fig. 10.b.

In the soil mesh in Fig. 16.a, the distance of the lateral boundary from the underground structure is greater than 5 times the structural width, which meets the requirements of the Chinese code [72]. As for the soil domain vertical dimension, 39.2 m was selected as engineering bedrock depth [32,33,37,39,55,56].

In the station modeling (Fig. 16.b, Fig. 16.c and Fig. 16.d), the central columns (Fig. 6) are represented by an equivalent continuous wall having the same initial (linear elastic) stiffness per unit length (gross moment of inertia) than the corresponding columns [13,56,73,74]. The steel longitudinal (vertical) reinforcement of the equivalent continuous wall is considered to have the same area than that of the actual columns. As the true continuous elements (side walls and top and bottom slabs), this fictitious continuous element is assumed to behave under plane strain condition.

The soil-structure contact behavior is simulated with the surface-to-surface interaction technique built in ABAQUS [70]. Regarding the normal contact, separation is allowed, while compressive stress is directly transmitted; tangential sliding is described with a Coulomb model with a friction coefficient equal to 0.4 [45]. This value is commonly suggested for this type of situations, particularly the modelling of Daikai station [45]; also, it has been calibrated with centrifuge shaking table tests [42].

Table 3
Fitting parameters of the site soil [55].

Parameter	Soil layer					
	1	2	3	4	5	6
A	1.20	1.20	1.20	1.15	1.15	1.20
B	0.40	0.47	0.47	0.33	0.33	0.47
γ_0	1.69	5.80	5.80	5.36	5.36	5.80

6.2.2. Soil constitutive model

The soil dynamic nonlinear behavior is represented by a nonlinear viscoelastic constitutive law [67–69] (modified Davidenkov model) combined with the classical Masing rules [75]. It is assumed that water pressure does not play a significant role in this case (i.e., there is no risk of liquefaction), and a linear equivalent strategy is used. This soil modelling has been chosen as being widely used [6,27,28,55,56].

The skeleton curve of the stress–strain relationship in the Davidenkov model is given by:

$$\tau(\gamma) = G\,\gamma = G_{\max}(1 - H(\gamma))\gamma \quad H(\gamma) = \left[\frac{(\gamma/\gamma_0)^{2B}}{1 + (\gamma/\gamma_0)^{2B}}\right]^{A} \tag{9}$$

In equation (9), γ is the soil shear strain, $\tau(\gamma)$ is the stress–strain relationship depicted by the skeleton curve $H(\gamma)$, G is the soil shear modulus, and $G_{\max}$ is its maximum value.

The variations of the soil stiffness and damping parameters with its shear strain are described in Fig. 17.

A, B and γ_0 are parameters that depend on soil properties [76]; their values (for each soil layer in Fig. 10.b) are presented in Table 3.

6.2.3. Concrete and steel constitutive models

The concrete nonlinear behavior is described with a plastic-damage model [77,78]. Damage is represented by the tensile and compressive damage factors ranging between 0 (no damage) and 1 (total damage); these factors are computed from the damage variables (d_t and d_c, respectively) defined as [67]:

$$d_t = \begin{cases} 1 - \rho_t\left(1.2 - 0.2x^5\right) & x \le 1 \\ 1 - \dfrac{\rho_t}{\alpha_t (x-1)^{1.7} + x} & x > 1 \end{cases} \quad d_c = \begin{cases} 1 - \dfrac{\rho_c\, n}{n - 1 + x^n} & x \le 1 \\ 1 - \dfrac{\rho_c}{\alpha_c (x-1)^2 + x} & x > 1 \end{cases} \tag{10}$$

In the left equation (10), ρ_t is the normalized concrete stress ($\rho_t = f_{t,r}/E_c\,\varepsilon_{t,r}$), x is the normalized concrete strain ($x = \varepsilon/\varepsilon_{t,r}$), and α_t is a parameter that characterizes the descending branch of the uniaxial tensile stress–strain curve; $f_{t,r}$ is the representative (characteristic) value of the uniaxial tensile strength, E_c is the concrete deformation modulus, $\varepsilon_{t,r}$ is the corresponding tensile strain, and ε is the concrete axial strain. In the right equation (10), $n = E_c\varepsilon_{c,r}/(E_c\varepsilon_{c,r} - f_{c,r})$, and the definition of the related parameters is similar as in d_t. The tensile and compressive uniaxial stress–strain curves of concrete are selected as in [55].

The following values of the concrete mechanical parameters are assumed [37,41,55]: density 2500 kg/m^3, Poisson ratio 0.2, deformation modulus E_c = 32.6 GPa, dilation angle 36.3°, eccentricity 0.1, compressive recovery parameter 1, tensile recovery parameter 0, $F_{b0}/f_{c0} = 1.16$, $K = 0.667$ and viscosity 10^{-5} Pa·s. The parameter F_{b0}/f_{c0} represents the ratio between biaxial compressive yield strength and uniaxial compressive yield strength, and K is the ratio between second stress invariants on tensile and compressive meridians.

The steel reinforcement is represented by a classical elastoplastic model without strain hardening; their parameters are: elastic modulus 200 GPa, yield stress 240 MPa, and Poisson ratio 0.3.

6.2.4. Boundary conditions

The whole numerical simulation is divided into two analyses: static (gravity) and dynamic (seismic); the boundary conditions for each of them are different.

- **Static analysis.** In the static calculation, the horizontal displacement of the lateral boundaries and the vertical displacement of the bottom boundary are restrained.
- **Dynamic analysis.** In the dynamic calculation, the bottom boundary transmits the seismic excitation (horizontal and vertical seismic motions); the nodes are constrained to move according to these input signals. In the lateral boundaries, the nodes are free to move horizontally and vertically, but kinematic tie constraints (i.e. equal displacements at the left and right boundaries) [79] are introduced in order to reduce the reflection waves. This approach achieves the same results than more complex methods (e.g., the silent boundary condition) but in a simpler way, thus being widely used [4,80–84]; in addition, it has been verified by centrifuge shaking table testing [42].

6.2.5. Mechanical model of the rubber bearings

As described in section 4 (Fig. 6 and Fig. 7), the low lateral stiffness of the station is attained by using elastomeric bearings to connect the main structural elements; their characteristics are selected in subsection

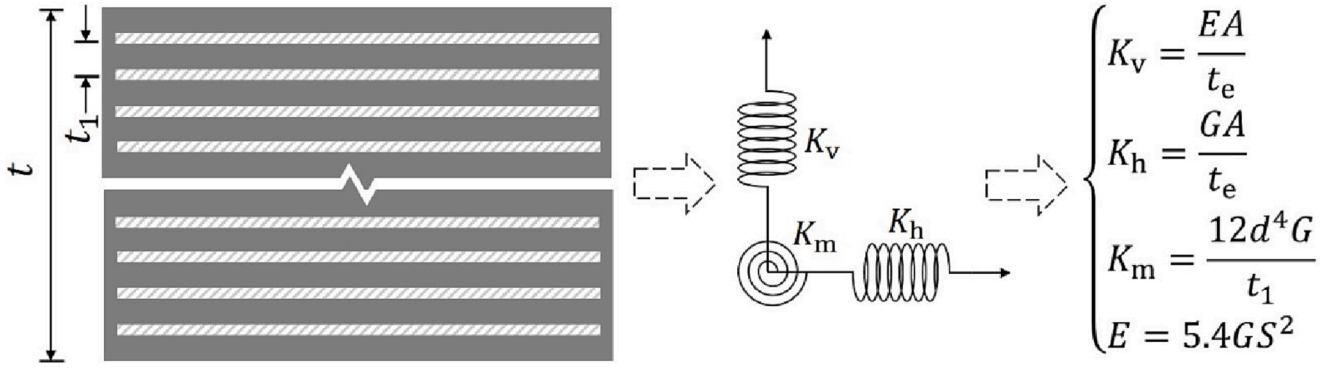

Fig. 18. Mechanical model of the circular bearings as the sliding-hinged components (solutions S1 and S2) [85].

Table 4
Mechanical properties of the bearings in the solutions S1 and S2 (Table 2).

Bearing	Compressive stiffness K_v (kN/m)	Shear stiffness K_h (kN/m)	Bending stiffness K_m (kNm/rad)	Bearing elastic modulus E (MPa)
Hinged bearings (structural joints)	301×10^3	679	12×10^3	443
Sliding bearing (central column)	512×10^3	1208	38×10^3	424

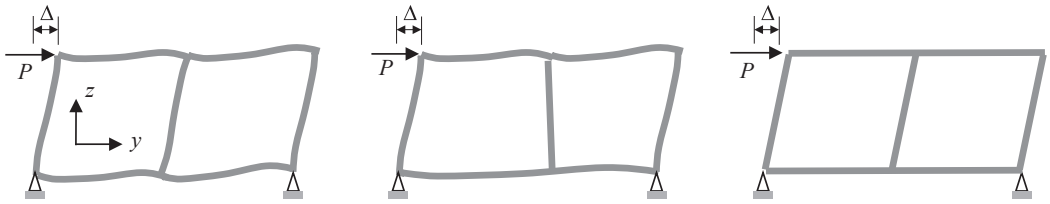

Fig. 19. Calculation of the transverse stiffness of solutions S0, S1 and S2.

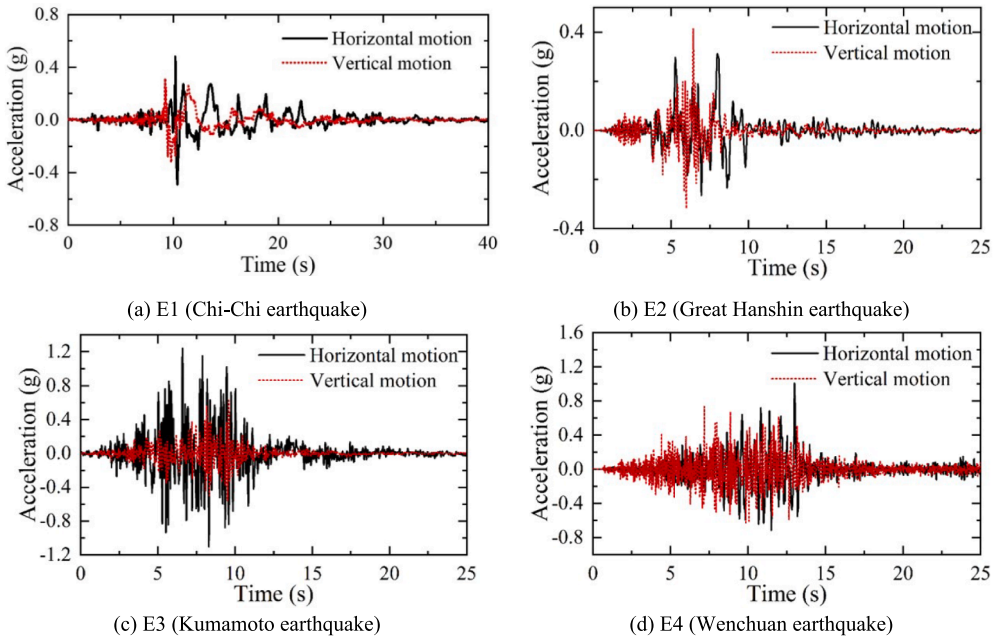

Fig. 20. Horizontal and vertical accelerograms of the E1, E2, E3 and E4 seismic inputs.

5.6 (Table 2). The elastomeric bearings consist of a rubber body with internal steel thin shims, as shown in Fig. 18; given that the rubber deformation modulus is rather low but its Poisson ratio is close to 0.5, the steel plates provide effective confinement, with a dramatic increase of the axial stiffness, but without compromising the shear flexibility and deformability. Elastomeric bearings are characterized by their simple fabrication, moderate cost, and easy installation, and have been widely used in civil engineering structures.

Fig. 18 shows that the bearings flexibility is described with axial, transverse and rotational springs; their stiffnesses are K_v, K_h and K_m, respectively. In Fig. 18, E is the rubber modulus of elasticity, G is the rubber shear modulus, A is the rubber bearing area, t_e is the total thickness of the rubber layers, t_1 is the thickness of a single rubber layer, d is the diameter of a circular bearing, and S is the bearing dimensionless shape factor (ratio between the effective loading area and the free side surface area). Table 4 displays the mechanical parameters of the bearings in Table 2; they are calculated according to the Chinese code [85].

6.2.6. Lateral stiffness of solutions S0 (Fig. 15.b), S1 (Fig. 15.c) and S2 (Fig. 15.d)

This subsection presents a comparison between the lateral stiffness of the three solutions S0, S1 and S2 (Daikai Station, Fig. 16.b, Fig. 16.c, Fig. 16.d). Such parameter is obtained, as suggested by [14], for the lone station (i.e. without the surrounding soil) considered as fixed in its bottom corners [14]; that configuration is described in Fig. 19.

As suggested in [14], the station stiffness is defined as the ratio between the concentrated lateral pushing force P and the racking displacement Δ; the corresponding linear static structural analysis is performed using the numerical model described in subsection 6.2.

The obtained results for solutions S0, S1 and S2 are 76.6 kN/mm, 63 kN/mm, and 24.6 kN/mm, respectively (per unit length). These values are expected, and show that the contribution of the central column is rather moderate (by comparing S0 and S1) and that the flexibilization introduced by the rubber bearings is important (by comparing S2 with S0 and S1). Noticeably, a specific design of such elements might have provided an ever lower stiffness of solution S2.

7. Selected seismic accelerograms for the time-history analyses

The input signals for the dynamic analyses are the four pairs of recorded seismic accelerograms displayed in Fig. 20.

Although most of the major international regulations for underground structures state that a larger number of accelerograms shall be taken for design, it should be kept in mind that the objective of this study is not to design any structure, but to assess preliminary the feasibility of the proposed solution. Moreover, most of the published works for Daikai and other underground stations consider typically four (or even less) inputs [80,86–89].

Fig. 20 shows that the four twosomes are referred as E1, E2, E3 and E4; each of them corresponds to horizontal and vertical components of actual earthquake records. Accelerograms E1, E3 and E4 belong to the Chi-Chi (1999, Taiwan China), Wenchuan (2008, Wenchuan China) and Kumamoto (2016, Kumamoto Japan) earthquakes; they are selected as are widely used in seismic analysis of underground structures because they have adversely affected such constructions. Accelerograms E2 belong to the Great Hanshin earthquake; were recorded at Kobe

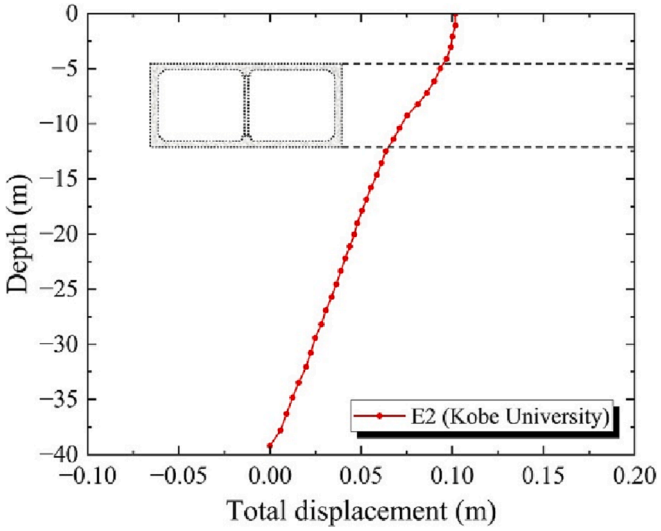

Fig. 21. Free-field soil deformation of the site soil obtained from the dynamic analysis under E2 input.

University seismological station [90]. As this seismic observatory is located on a rock outcrop near Daikai Station, the recorded accelerograms are considered close to those that actually shook the station. Detailed information on these ground motions can be found in [91].

Plots in Fig. 20 show up the relevance of the vertical components of the seismic ground motion, particularly in the Kobe earthquake (E2).

8. Time-history analyses for solutions S0, S1 and S2 and inputs E1-E4

8.1. Analyses performed

The nonlinear time-history analyses are carried out for solutions S0 (Fig. 16.b), S1 (Fig. 16.c) and S2 (Fig. 16.c) undergoing inputs E1 (Fig. 20.a), E2 (Fig. 20.b), E3 (Fig. 20.c) and E4 (Fig. 20.d). The analyses are performed using an implicit formulation. The time step is variable along the input duration, ranging between 0.02 and 0.00001 s. Second order effects are accounted for, mainly to reproduce the buckling of the central column.

8.2. Results of soil and structure transverse deformation

Fig. 21 displays the free-field soil deformation of the site soil in the dynamic analysis under E2 input. The plotted deformation corresponds to the moment when the relative displacement between the ceiling and bottom slabs of the station is maximum.

Comparison between Fig. 10 and Fig. 21 shows a rather satisfactory agreement.

Fig. 22 displays the time-history responses of the drift ratio of the side walls (left plots, Fig. 22.a, Fig. 22.c, Fig. 22.e, Fig. 22.g) and the central column (right plots, Fig. 22.b, Fig. 22.d, Fig. 22.f, Fig. 22.h) excited by the simultaneous actuation of the pairs of seismic accelerograms E1-E4 (Fig. 20). The drift ratio of the walls has been obtained by dividing the relative displacement between the ceiling and floor slabs by 6.76 m (distance between their center lines, Fig. 4.b); regarding the column, its drift ratio is the relative displacement between their top and bottom sections divided by its height (3.42 m in solution S0, Fig. 4.b, and 3.13 m in solutions S1 and S2, Fig. 11).

Fig. 22 provides the following major remarks:

- The performances for inputs E1-E4 are pretty analogous; this broadly confirms that the conclusions derived are deeply grounded.
- Left plots show that the initial drift behaviors of the external walls exhibit some degree of similarity for the three solutions (S0, S1 and S2); this apparently corroborates that the seismic response of underground structures is basically dominated by the imposed free-field soil strain [3]. Conversely, the permanent displacements are different, their values being apparently random [92,93]; this trend might be due to the complex interaction between the decaying nonlinear behaviors of soil and structure. Given the low lateral stiffness of solution S2, it might be expected a higher permanent displacement; conversely, solution S2 results in less permanent displacements in most of the cases.
- Right plots show that, as expected, the drift of the central column in solutions S1 and S2 is near zero.
- Comparison between left and right plots shows that the lateral displacements of the central column and walls in solution S0 are alike.

Contrast between Fig. 22.c and subsection 5.7 shows that the maximum demand drift ratios predicted in this paper by the simplified formulation in [14] (equation (8)) are greater than the values obtained from the nonlinear dynamic analyses (Fig. 22.c, corresponding to the input that actually excited the structure). This trend corroborates that, as expected, the simplified Wang formulation can be rather conservative [94].

8.3. Results of internal forces

Fig. 23 displays, for solutions S0, S1 and S2, the maximum internal forces (axial and shear forces, and bending moment) in any section of the structural members (walls, slabs and central column) during the seismic excitation with inputs E1-E4.

Fig. 23 provides the following major remarks:

- All the results correspond to peak values that do not necessarily belong to the same instant or to the same section; this produces highly random values [92,93].
- As expected, the shear force and bending moment in the central column are almost zero in solutions S1 and S2.
- About walls and slabs, the internal forces in S1 are generally higher than in S0, seemingly due to the lack of structural cooperation of the central column; conversely, the internal forces in S2 are significantly reduced.

Comparison between Fig. 23.b for solution S2 and Fig. 15 (approximate static equivalent analysis) shows rather comparable results. The most remarkable differences can be explained by the aforementioned important randomness of the peak results, the conservativeness of the simplified static analysis, and the nonlinear structural behavior assumed in the analysis whose results are displayed in Fig. 23.

8.4. Results of damage factors

Fig. 24 displays the tensile and compressive damage factors (DAMAGET and DAMAGEC, respectively) for solutions S0, S1 and S2 under the seismic input E2. Results for inputs E1, E3 and E4 exhibit basically the same trends.

Fig. 24 provides regular and expected remarks:

- **Central column**. There is no damage in solutions S1 and S2, but in solution S0 both member ends are severely damaged (due to bending, obviously).
- **Walls and slabs**. Damage is significantly alleviated in the proposed solution S2, and follows expected patterns (basically, concentration at sections with maximum bending moments).

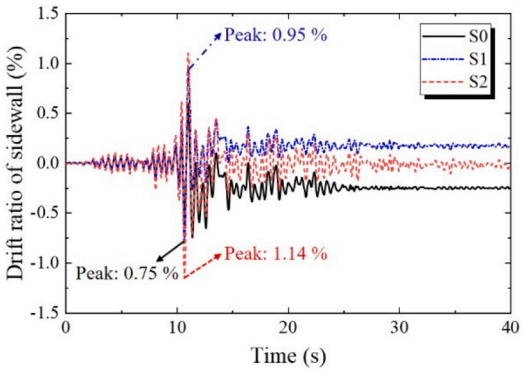

(a) Sidewalls. Seismic input E1

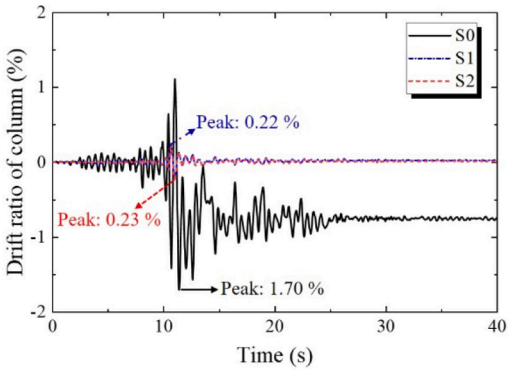

(b) Central column. Seismic input E1

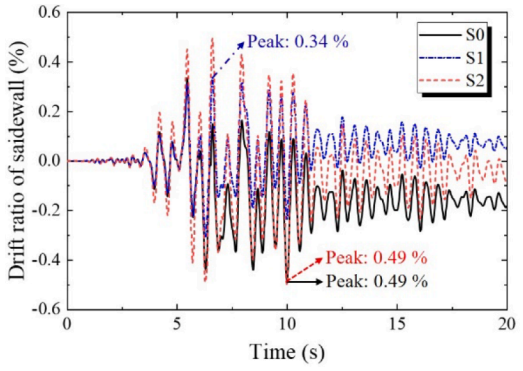

(c) Sidewalls. Seismic input E2

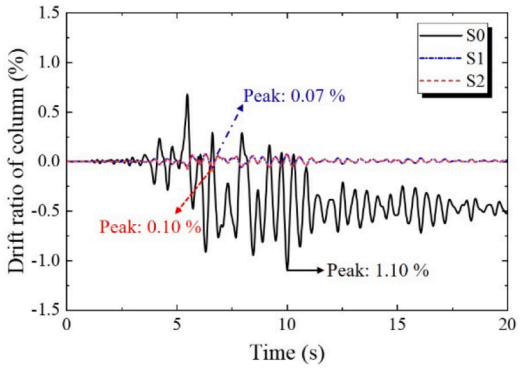

(d) Central column. Seismic input E2

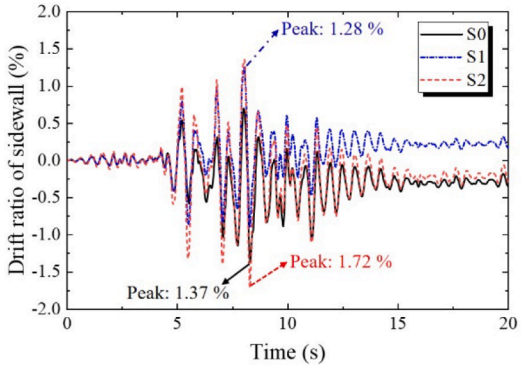

(e) Sidewalls. Seismic input E3

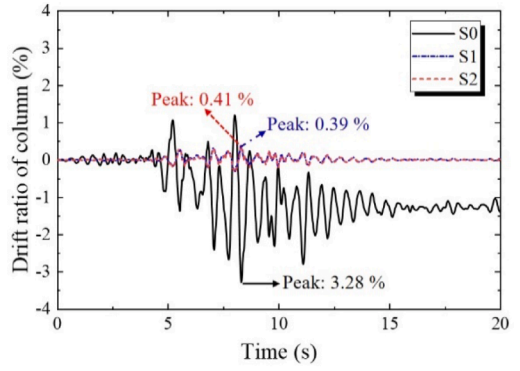

(f) Central column. Seismic input E3

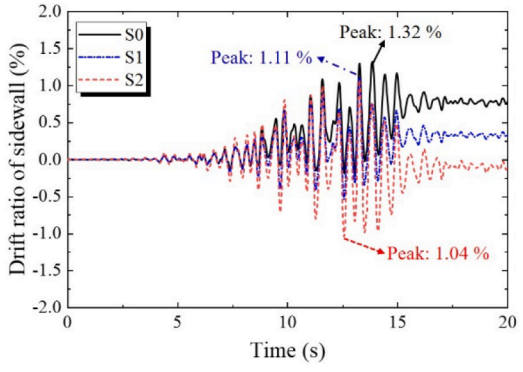

(g) Sidewalls. Seismic input E4

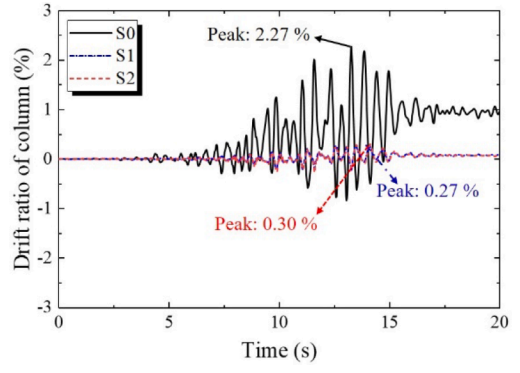

(h) Central column. Seismic input E4

Fig. 22. Time-history results of the drift ratio in the Daikai Station in solutions S0, S1 and S2.

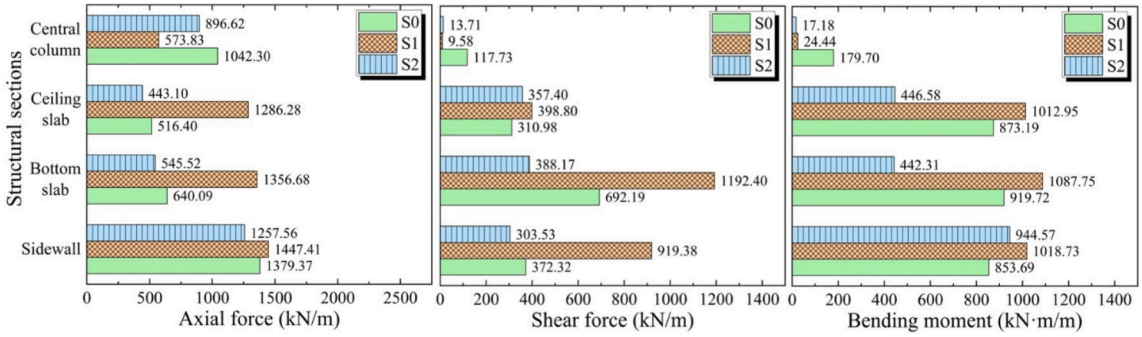

(a) Seismic input E1

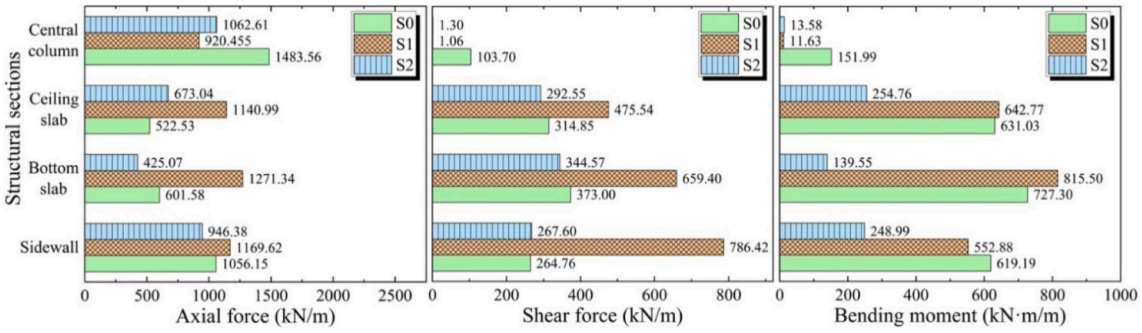

(b) Seismic input E2

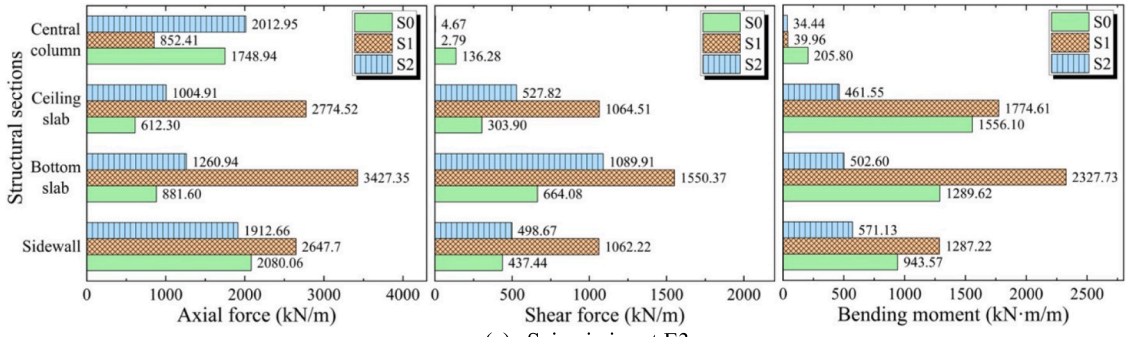

(c) Seismic input E3

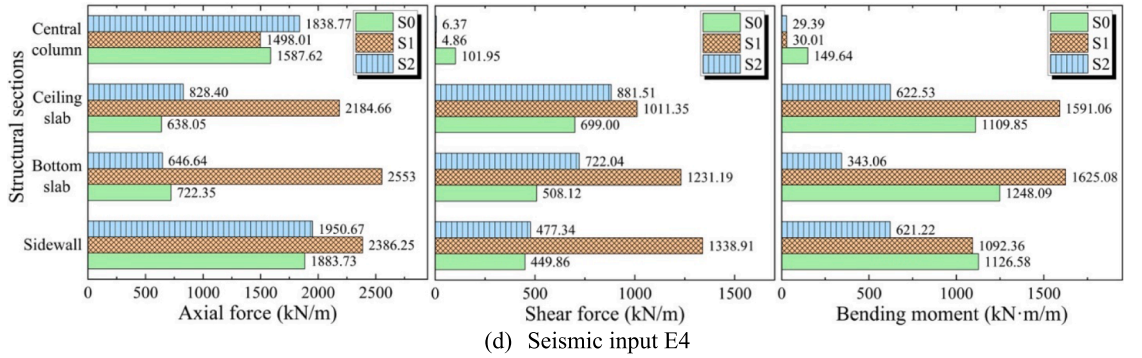

(d) Seismic input E4

Fig. 23. Comparison between the peak internal forces in solutions S0, S1 and S2.

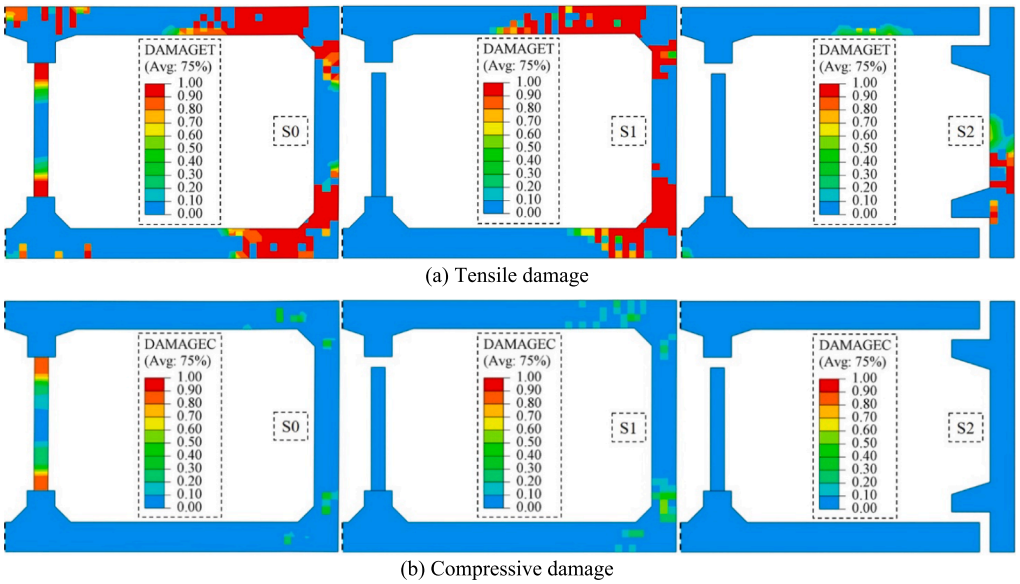

(a) Tensile damage

(b) Compressive damage

Fig. 24. Comparison between damage performance of solutions S0, S1 and S2. Seismic input E2.

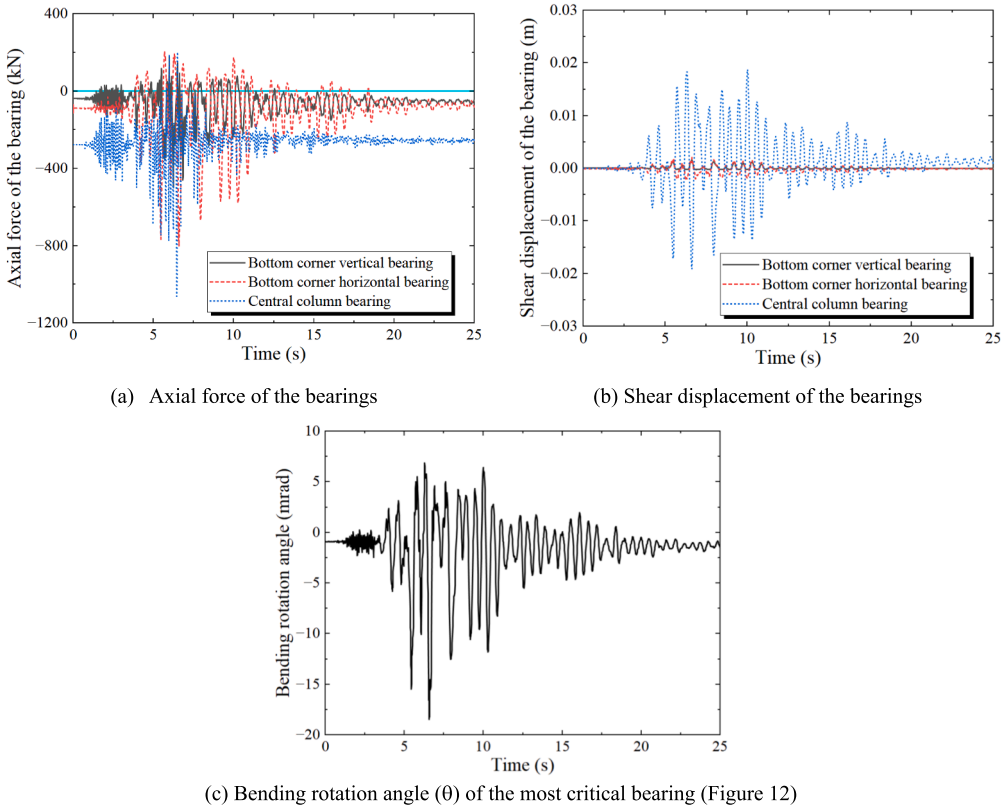

(a) Axial force of the bearings

(b) Shear displacement of the bearings

(c) Bending rotation angle (θ) of the most critical bearing (Figure 12)

Fig. 25. Time-history results of the rubber bearings in solution S2 for input E2.

- **All elements.** Comparison between Fig. 24.a and Fig. 24.b shows that, for S0, S1 and S2, the tensile damage is higher. This trend is due to the larger concrete compressive strength, this circumstance being partially compensated by the greater compressive stress.

Fig. 22, Fig. 23 and Fig. 24 show that the superiority of S2 over S1 is not expressed in terms of drift histories, but internal forces and damage factors.

8.5. *Results for rubber bearings*

Fig. 25.a and Fig. 25.b display, for input E2 and for the most representative rubber bearings, time-history results of axial force and shear displacement, respectively; in Fig. 25.a, positive values indicate tension. Fig. 25.c presents the bending rotation angle (θ) of a rubber bearing of the bottom left corner (Fig. 12).

Comparison between Table 2 and Fig. 25 shows that the demands on the bearings are clearly below their capacity. The tensile axial force

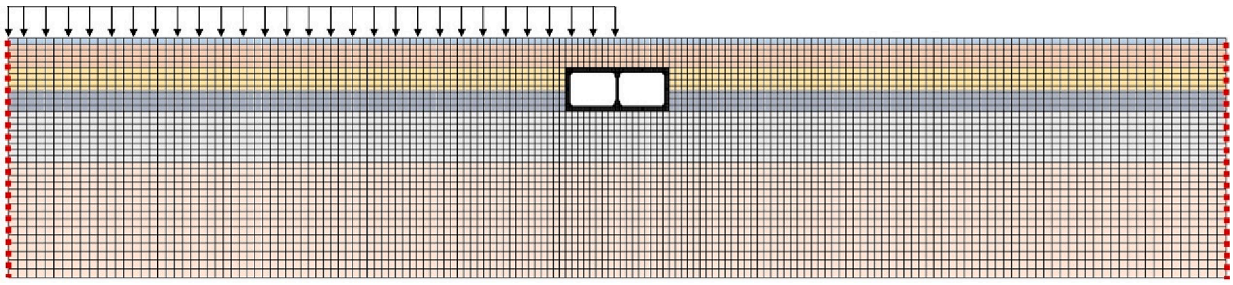

Fig. 26. Asymmetric gravity loading (solutions S0, S1 and S2).

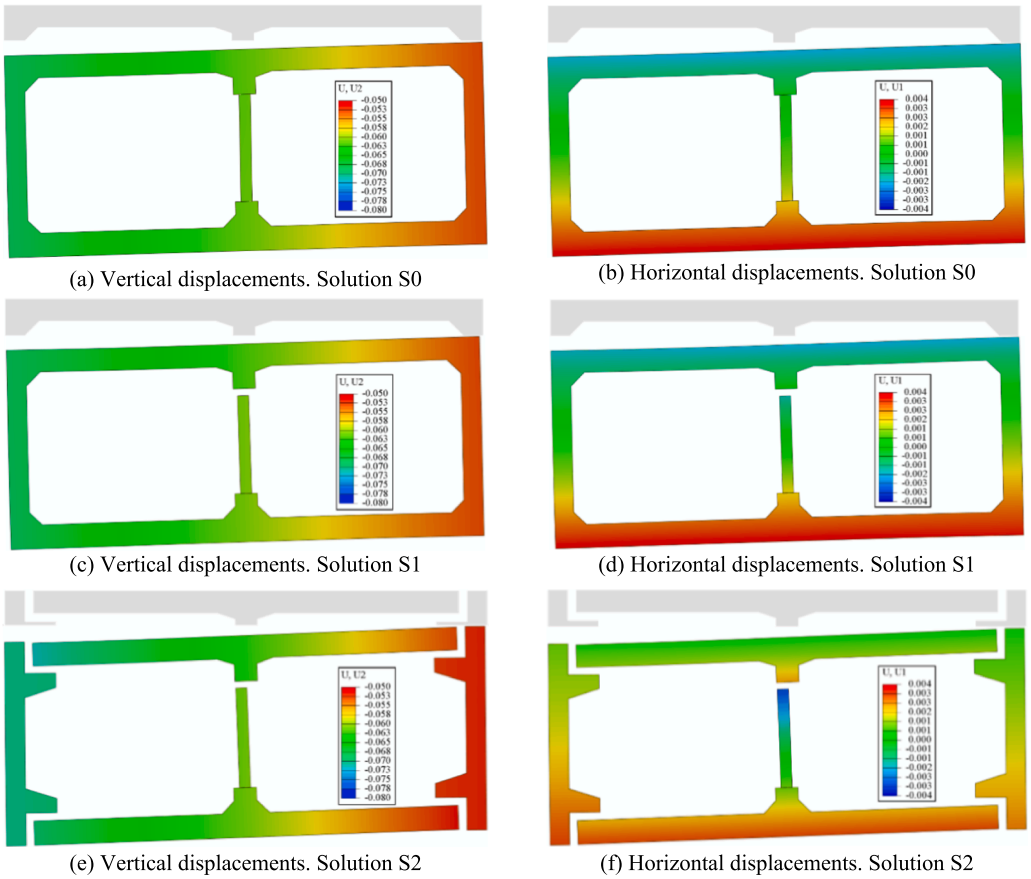

(a) Vertical displacements. Solution S0

(b) Horizontal displacements. Solution S0

(c) Vertical displacements. Solution S1

(d) Horizontal displacements. Solution S1

(e) Vertical displacements. Solution S2

(f) Horizontal displacements. Solution S2

Fig. 27. Deformation of the Daikai Station (solutions S0, S1 and S2) due to gravity asymmetric loading (unit: m, scale factor of displacement: 30).

observed in Fig. 25.a (approximately, 200 kN) leads to an average tensile stress of 200,000 / ($\pi \times 150^2$) = 2.83 MPa; this value is well below the natural rubber tensile strength of 18 MPa [95]. On the other hand, this tensile force can be easily resisted by any common bolted connection with the concrete members. Finally, Fig. 25.c shows that the bending rotation angle is small; therefore, no relevant interaction between axial force and bending moment can be expected.

9. Conclusions

This paper proposes a rather innovative structural solution for cut-and-cover shallow underground stations and tunnels: instead of conventional rigid box sections, the connections between the main structural elements (walls, slabs and columns) are either hinged or sliding, in order to obtain a section with low lateral stiffness. This approach is suitable for both cast-in-place and precast constructions. The main advantage of this solution is its almost total insensitivity to transverse seismic excitations.

The suitability of the offered solution is verified by applying it to a relevant case study: Daikai Station (Kobe, Japan), severely damaged by the 1995 Great Hanshin Earthquake. An alternative solution in which the major structural members are connected through flexible rubber bearings is carefully designed. A detailed study of this particular case is performed; it includes the construction process (cast on site), water tightness, and, mainly, mechanical resistance to gravity and seismic effects. Regarding the latter topic, two types of seismic structural analysis are performed: simplified static calculations (handmade) and complex 2-D advanced nonlinear dynamic analyses (for four representative pairs of horizontal and vertical recorded seismic accelerograms) using advanced finite element models of the station and the surrounding soil; the agreement between both calculations is satisfactory. These static and dynamic analyses have been performed in the proposed (flexible) solution with hinged or sliding connections, and in the traditional solution with rigid connections. These studies provide better results for the flexible proposed solution in terms of permanent racking displacements in the station section, internal forces and damage factors

in the structural members, and stresses and strains in the rubber bearings. These comparisons confirm the superior seismic performance of the proposed alternative solution.

On the other hand, the technical feasibility of the proposed construction solution is further corroborated by the relatively common use of hinged connections in actual underground stations, mostly to facilitate the construction.

The same authors have performed a supplementary case study on a 2-story 3-bay subway station located in China. The positive results obtained in both researches provide additional validation of the proposed constructive solution.

Further research includes numerical parametric studies (aimed to cover a wider range of situations), and field and laboratory experimental verification, among other relevant topics.

CRediT authorship contribution statement

Xiangbo Bu: Methodology, Software, Writing – review & editing. **Alberto Ledesma:** Validation, Writing – review & editing. **Francisco López-Almansa:** Conceptualization, Writing – original draft.

Declaration of Competing Interest

The authors declare that they have no known competing financial interests or personal relationships that could have appeared to influence the work reported in this paper.

Data availability

Data will be made available on request.

Acknowledgements

This research has been partially funded by the Spanish Research Agency (AEI) of the Ministry of Science and Innovation (MICIN) through project with reference: PID2020-117374RB-I00 / AEI / 10.13039/501100011033. The study of Mr. Xiangbo Bu in the Technical University of Catalonia (UPC-BarcelonaTech) is funded by Chinese Government Scholarship (CSC No. 201906560013). These supports are gratefully acknowledged.

Appendix

Static non-seismic analysis for asymmetric loading

In order to further validate the capacity of the proposed solution S2 to resist unbalanced loading, this appendix presents an additional static non-seismic analysis for asymmetric gravity loads; the analysis is performed with the formulation described in subsection 6.2. Fig. 26 displays the loading acting only on the left half of the analyzed model (Fig. 16).

In Fig. 26, the additional load is equal to 22 kN/m^2; this value is the actual design load [31].

Fig. 27 displays the deformed configurations of solutions S0, S1 and S2 of the Daikai Station under the gravity asymmetric loading depicted in Fig. 26. Displacements are in m, and the scale factor is 30.

Fig. 27 shows that the lateral and vertical displacements are rather similar for the three solutions, thus indicating that the small lateral stiffness of solution S2 (subsection 6.2.6) does not have a strong effect in case of asymmetrical loading. On the other hand, Fig. 27.a, Fig. 27.c and Fig. 27.e show that the asymmetric ground loading results into a significant structural differential settlement, which reveals the importance of the vertical load in Fig. 26.

List of acronyms

E1/E2/E3/E4: Pairs of seismic accelerograms (Fig. 20).
HDRB: High-Damping Rubber Bearing (subsection 4.1).
PVC: PolyVinyl Chlorid (subsection 4.3).
S0/S1/S2: Conventional (rigid)/intermediate/low stiffness solutions for the Daikai Station (Fig. 16, Fig. 19).

List of symbols

A: Rubber bearing area (Fig. 18).
A/B: Exponents to be determined by fitting experimental results (equation (9)).
$a_1/a_2/a_3/a_4/a_5$: Height (thickness, gap) of the rubber bearings (Fig. 11, Table 1 and Table 2, equations (2) and (3)).
$b/c/d$: Dimensions of the proposed solution (Fig. 11, equation (4)).
d: Diameter of a circular bearing (Fig. 18).
d_c/d_t: Compressive/tensile damage variables (equation (10)).
E/G: Bearing elastic/shear modulus (Fig. 18, Table 4).
$F_0/F_1/F_2$: Flexibility ratio (quotient between the soil shear stiffness and the tunnel racking stiffness, equation (5)) for solutions S0/S1/S2.
f: Frequency (Hz) (subsection 6.2.1).
G/G_{max}: Soil shear modulus/its maximum value (equation (9)).
$K_v/K_h/K_m$: Compressive/shear/bending stiffness of the rubber bearings (Fig. 18, Table 4).
l: Length of the cantilevers (brackets) and the interposed segments (Fig. 6.c, equation (4)).
M_w: Moment magnitude of a given earthquake (subsection 3.1).
n: Exponent (equation (10)).
P: Concentrated lateral pushing force (Fig. 19).
$R_0/R_1/R_2$: Racking coefficient (ratio between the racking and free-field displacements) for solutions S0/S1/S2.
S: Bearing dimensionless shape factor (Fig. 18).
t_e/t_1: Total thickness of the rubber layers/thickness of a single rubber layer (Fig. 18).
v_s: Shear wave velocity (subsection 6.2.1).
$w_1/w_2/w_3/w_4/w_5$: Width of the rubber bearings (Fig. 11, Table 2).
x: Normalized concrete strain (equation (10)).
$x/y/z$: Longitudinal/transverse/vertical coordinates.
α_c/α_t: Parameters that characterize the descending branch of the compressive/tensile stress–strain curves (equation (10)).
$\Delta_0/\Delta_1/\Delta_2$: Racking deformation (displacement) of the structure (Fig. 7, Fig. 13, Fig. 19, equations (1), (3) and (7)) for solutions S0/S1/S2.
Δ_{FF}: Free-field displacement of the soil (subsection 5.2 and 5.7).
ϕ: Diameter of a reinforcement bar (Fig. 3).
γ/γ_0: Soil shear strain/its fitting value (equation (9)).
$\gamma_1/\gamma_2/\gamma_3/\gamma_4/\gamma_5$: Shear strain in the rubber bearings (Fig. 11, Table 1 and Table 2, equations (2) and (3)).
λ: Shear wave length (subsection 6.2.1).
ρ_c/ρ_t: Compressive/tensile normalized concrete stress (equation (10)).
$\theta_0/\theta_1/\theta_2$: Rotation angle of the wall with respect to the slab (Fig. 7, Fig. 12, Fig. 25, Table 1 and Table 2, equations (1) and (2)) for solutions S0/S1/S2.
τ: Soil shear stress (equation (9)).

References

[1] Huang Z-K, Zhang D-M. Scalar-and vector-valued vulnerability analysis of shallow circular tunnel in soft soil. Transp Geotech 2021;27:100505.
[2] International Association of Public Transport (UITP). World metro figures 2018. International Association of Public Transport. Brussels: 2018.
[3] Hashash YMA, Hook JJ, Schmidt B, John I, Yao C. Seismic design and analysis of underground structures. Tunn Undergr Sp Technol 2001;16:247–93.
[4] Tsinidis G, Pitilakis K, Madabhushi G. On the dynamic response of square tunnels in sand. Eng Struct 2016;125:419–37.
[5] Huang Z, Argyroudis SA, Pitilakis K, Zhang D, Tsinidis G. Fragility assessment of tunnels in soft soils using artificial neural networks. Underground Space 2022;7(2):242–53.

[6] Liu H, Xu C, Du X. Seismic response analysis of assembled monolithic subway station in the transverse direction. Eng Struct 2020;219:110970.
[7] Liu H, Wang Z, Du X, Shen GQP. The seismic behaviour of precast concrete interior joints with different connection methods in assembled monolithic subway station. Eng Struct 2021;232:111799.
[8] Kim DS, Konagai K. Seismic isolation effect of a tunnel covered with coating material. Tunn Undergr Sp Technol 2000;15(4):437–43.
[9] Kim D-S, Konagai K. Key parameters governing the performance of soft tunnel coating for seismic isolation. Earthq Eng Struct Dyn 2001;30(9):1333–43.
[10] Chen ZY, Shen H. Dynamic centrifuge tests on isolation mechanism of tunnels subjected to seismic shaking. Tunn Undergr Sp Technol 2014;42:67–77.
[11] Zheng Y, Yue C. Shaking table test study on the functionality of rubber isolation bearing used in underground structure subjected to earthquakes. Tunn Undergr Sp Technol 2020;98:103153.
[12] Chen Z-Y, Chen W, Bian G-Q. Seismic performance upgrading for underground structures by introducing shear panel dampers. Adv Struct Eng 2014;17(9):1343–57.
[13] Xu Z, Du X, Xu C, Han R. Numerical analyses of seismic performance of underground and aboveground structures with friction pendulum bearings. Soil Dyn Earthq Eng 2020;130:105967.
[14] Wang JN. Seismic design of tunnels: a state-of-the-art approach, monograph, monograph 7. Brinckerhoff, Quade Douglas Inc, New York: Parsons; 1993.
[15] Sharma S, Judd WR. Underground opening damage from earthquakes. Eng Geol 1991;30(3-4):263–76.
[16] Richardson AM, Blejwas TE. Seismic design of circular-section concrete-lined underground openings: Preclosure performance considerations for the Yucca Mountain Site. Sandia National Lab. Albuquerque, NM (United States): (SNL-NM); 1992.
[17] Ding X, Feng Li, Wang C, Chen Z, Han L. Shaking table tests of the seismic response of a utility tunnel with a joint connection. Soil Dyn Earthq Eng 2020;133:106133.
[18] Qiao Y, Tang J, Liu G, He M. Longitudinal mechanical response of tunnels under active normal faulting. Underground Space 2022;7(4):662–79.
[19] Rodríguez Sánchez J, Díaz-Moreno AJ, Martínez-Ruiz GHI. Seismic design of the mercado santa anita station in L2 Metro Lima Project. ACHE, A Coruña, Spain: VII Conf; 2019.
[20] Nakamura S, Yoshida N, Iwatate T. Damage to Daikai subway station during the 1995 Hyogoken-Nambu earthquake and its investigation. Japan Soc Civ Eng Comm Earthq Eng 1996;6:287–95.
[21] Iida H, Hiroto T, Yoshida N, Iwafuji M. Damage to Daikai subway station. Soils Found 1996;36:283–300.
[22] Yamato T, Umehara T, Aoki H, Nakamura S, Ezaki J, Suetomi I. Damage to Daikai subway station of Kobe rapid transit system and estimation of its reason during the 1995 Hyogoken-Nanbu earthquake. Doboku Gakkai Ronbunshu 1996;1996(537):303–20.
[23] Chung RM. January 17, 1995 Hyogoken-Nanbu (Kobe) earthquake: Performance of structures, lifelines, and fire protection systems (NIST SP 901) 1996.
[24] Bu X, Ledesma A, López-Almansa F. Novel seismic design solution for underground structures. case study of a 2-story 3-bay subway station. Soil Dyn Earthq Eng 2022;153:107087.
[25] Yang X, Lin F. Prefabrication technology for underground metro station structure. Tunn Undergr Sp Technol 2021;108:103717.
[26] Tao L, Ding P, Yang X, Lin P, Shi C, Bao Y, et al. Comparative study of the seismic performance of prefabricated and cast-in-place subway station structures by shaking table test. Tunn Undergr Sp Technol 2020;105:103583.
[27] Chen J, Xu C, El Naggar HM, Du X. Study on seismic performance and index limits quantification for prefabricated subway station structures. Soil Dyn Earthq Eng 2022;162:107460.
[28] Chen J, Xu C, El Naggar HM, Du X. Seismic response analysis of rectangular prefabricated subway station structure. Tunn Undergr Sp Technol 2023;131:104795.
[29] Owen GN, Scholl RE. Earthquake engineering of large underground structures 1981.
[30] Scawthorn C, Yanev PI. 17 January 1995, Hyogo-ken Nambu. Japanese earthquake Eng Struct 1995;17(3):146–57.
[31] Yoshida N, Nakamura S, Iwafuji M, YOSHIMURA H. Survey and restoration of the Daikai Subway Station damaged during the Hyogoken-Nanbu earthquake. Tunn Ouvrages Souterr 1995;1996:363–71.
[32] Lu C-C, Hwang J-H. Nonlinear collapse simulation of Daikai Subway in the 1995 Kobe earthquake: Necessity of dynamic analysis for a shallow tunnel. Tunn Undergr Sp Technol 2019;87:78–90.
[33] Nguyen V-Q, Nizamani ZA, Park D, Kwon O-S. Numerical simulation of damage evolution of Daikai station during the 1995 Kobe earthquake. Eng Struct 2020;206:110180.
[34] Uenishi K, Sakurai S. Characteristic of the vertical seismic waves associated with the 1995 Hyogo-ken Nanbu (Kobe), Japan earthquake estimated from the failure of the Daikai Underground Station. Earthq Eng Struct Dyn 2000;29(6):813–21.
[35] Samata S, Ohuchi H, Matsuda T. A study of the damage of subway structures during the 1995 Hanshin-Awaji earthquake. Cem Concr Compos 1997;19(3):223–39.
[36] Ma XF, Mochizuki A. Damage and restoration of the collapsed daikai subway satation during the hyogoken-nambu earthquake. J Railw Eng Soc 1998:446–52.
[37] Ma C, Lu D-C, Du X-L, Qi C-Z, Zhang X-Y. Structural components functionalities and failure mechanism of rectangular underground structures during earthquakes. Soil Dyn Earthq Eng 2019;119:265–80.
[38] Sayed MA, Kwon O-S, Park D, Van Nguyen Q. Multi-platform soil-structure interaction simulation of Daikai subway tunnel during the 1995 Kobe earthquake. Soil Dyn Earthq Eng 2019;125:105643.
[39] Xu Z, Du X, Xu C, Hao H, Bi K, Jiang J. Numerical research on seismic response characteristics of shallow buried rectangular underground structure. Soil Dyn Earthq Eng 2019;116:242–52.
[40] Xu Z, Du X, Xu C, Jiang J, Han R. Simplified equivalent static methods for seismic analysis of shallow buried rectangular underground structures. Soil Dyn Earthq Eng 2019;121:1–11.
[41] Dong R, Jing L, Li Y, Yin Z, Wang G, Xu K. Seismic deformation mode transformation of rectangular underground structure caused by component failure. Tunn Undergr Sp Technol 2020;98:103298.
[42] Xu C, Zhang Z, Li Y, Du X. Validation of a numerical model based on dynamic centrifuge tests and studies on the earthquake damage mechanism of underground frame structures. Tunn Undergr Sp Technol 2020;104:103538.
[43] Sandoval E, Bobet A. The undrained seismic response of the Daikai Station. Tunn Undergr Sp Technol 2020;103:103474.
[44] An X, Shawky AA, Maekawa K. The collapse mechanism of a subway station during the Great Hanshin earthquake. Cem Concr Compos 1997;19(3):241–57.
[45] Huo H, Bobet A, Fernández G, Ramírez J. Load transfer mechanisms between underground structure and surrounding ground: evaluation of the failure of the Daikai station. J Geotech Geoenviron Eng 2005;131(12):1522–33.
[46] Parra-Montesinos GJ, Bobet A, Ramirez JA. Evaluation of soil-structure interaction and structural collapse in Daikai subway station during Kobe earthquake. ACI Mater J 2006;103:113.
[47] Yu H, Li X. Investigation on damage mechanism of the Daikai station induced by the strong Kobe earthquake. Int J Earth Environ Sci 2017;2:10.
[48] Du X-L, Li Y, Xu C-S, Lu DC, Xu ZG, Jin L. Review on damage causes and disaster mechanism of Daikai subway station during 1995 Osaka-Kobe Earthquake. Chinese J Geotech Eng 2018;40:223–36.
[49] Li W, Chen Q. Seismic performance and failure mechanism of a subway station based on nonlinear finite element analysis. KSCE J Civ Eng 2018;22(2):765–76.
[50] Lu D, Wu C, Ma C, Du X, El Naggar MH. A novel segmental cored column for upgrading the seismic performance of underground frame structures. Soil Dyn Earthq Eng 2020;131:106011.
[51] Mikami A, Konagai K, Sawada T. Stiffness design of isolation rubber for center columns of tunnel. Doboku Gakkai Ronbunshu 2001;2001:415–20.
[52] Chen Z-Y, Zhao Hu, Lou M-L. Seismic performance and optimal design of framed underground structures with lead-rubber bearings. Struct Eng Mech An Int J 2016;58(2):259–76.
[53] Lianjin T, Junhai A, Nan G. Isolation effect analysis on bidirectional RFPS bearing applied in the metro stations engineering. J Earthq Eng Eng Vib 2016;36:52–8.
[54] Ma C, Lu D, Du X. Seismic performance upgrading for underground structures by introducing sliding isolation bearings. Tunn Undergr Sp Technol 2018;74:1–9.
[55] Liu Di, Du X, El Naggar HM, Xu C, Chen Q. Seismic mitigation performance analysis of underground subway station with arc grooved roller bearings. Soil Dyn Earthq Eng 2022;153:107082.
[56] Liu Di, Xu C, Du X, Naggar HME, Jiang J. Seismic performance and fragility analysis of underground subway station with rubber bearings. Soil Dyn Earthq Eng 2022;162:107511.
[57] Wang Y, Chen Q, Zhao Z, He Z. A resilient column with angular friction damper for seismic performance upgrading of underground structures. Tunn Undergr Sp Technol 2021;116:104085.
[58] Jing Y, Haiyang Z, Wei W, Zhenghua Z, Guoxing C. Seismic performance and effective isolation of a large multilayered underground subway station. Soil Dyn Earthq Eng 2021;142:106560.
[59] He Z, Chen Q. Upgrading the seismic performance of underground structures by introducing lead-filled steel tube dampers. Tunn Undergr Sp Technol 2021;108:103727.
[60] Ma C, Lu D, Gao H, Du X, Qi C. Seismic performance improvement of underground frame structures by changing connection type between sidewalls and slab. Soil Dyn Earthq Eng 2021;149:106851.
[61] Grantz W, Tan L, Sørensen E, Burger H, Gursoy A, Ingerslev C. Chapter 4 waterproofing and maintenance. Tunn Undergr Space Technol 1997;12(2):111–24.
[62] Gokce A, Koyama F, Tsuchiya M, Gencoglu T. The challenges involved in concrete works of Marmaray immersed tunnel with service life beyond 100 years. Tunn Undergr Sp Technol 2009;24(5):592–601.
[63] Hu Z, Xie Y, Wang J. Challenges and strategies involved in designing and constructing a 6 km immersed tunnel: a case study of the Hong Kong–Zhuhai–Macao Bridge. Tunn Undergr Sp Technol 2015;50:171–7.
[64] Gong C, Ding W, Soga K, Mosalam KM. Failure mechanism of joint waterproofing in precast segmental tunnel linings. Tunn Undergr Sp Technol 2019;84:334–52.
[65] Zhang J-L, Liu X, Zhao J-B, Yuan Y, Mang H. Application of a combined precast and in-situ-cast construction method for large-span underground vaults. Tunn Undergr Sp Technol 2021;111:103795.
[66] GB 50011-2010. Code for Seismic Design of Buildings. Beijing, China: China Architecture and Building Press: 2010.
[67] GB 50010-2010. GB 50010-2010 Code for design of concrete structures. Beijing: China Architecture and Building Press; 2010.
[68] Kim K, Giacalone C, Elgamal A, Shing PB. Racking response of reinforced concrete cut and cover tunnel. California Dept of Transportation 2016.
[69] Penzien J. Seismically induced racking of tunnel linings. Earthq Eng Struct Dyn 2000;29(5):683–91.
[70] Abaqus. Abaqus. 6.16 Documentation (Abaqus), 2016. Abaqus User's Guid 2016 2016. http://130.149.89.49:2080/v2016/index.html.

[71] Kuhlemeyer RL, Lysmer J. Finite element method accuracy for wave propagation problems. J Soil Mech Found Div 1973;99(5):421–7.
[72] GB50909-2014. Code for seismic design of urban rail transit structures. China Planning Press, Beijing; 2014.
[73] Su C, Baizan T, Haiyang Z, Jianning W, Xiaojun Li, Kai Z. Experimental investigation of the seismic response of shallow-buried subway station in liquefied soil. Soil Dyn Earthq Eng 2020;136:106153.
[74] Zhuang H, Yang J, Chen S, Dong Z, Chen G. Statistical numerical method for determining seismic performance and fragility of shallow-buried underground structure. Tunn Undergr Sp Technol 2021;116:104090. https://doi.org/10.1016/j.tust.2021.104090.
[75] Zhuang H, Guo-xing C, Liang Y. A developed dynamic viscoelastic constitutive relations of soil and implemented by ABAQUS software. Rock Soil Mech 2007;28:436–42.
[76] Zhuang H. Study on nonlinear dynamic soil-underground structure interaction and its large-size shaking table test. Nanjing, China: Nanjing University of Technology; 2006.
[77] Lee J, Fenves GL. Plastic-damage model for cyclic loading of concrete structures. J Eng Mech 1998;124(8):892–900.
[78] Lubliner J, Oliver J, Oller S, Oñate E. A plastic-damage model for concrete. Int J Solids Struct 1989;25(3):299–326.
[79] Zienkiewicz OC, Bicanic N, Shen FQ. Earthquake input definition and the trasmitting boundary conditions. Adv. Comput. nonlinear Mech.: Springer; 1989. p. 109–38.
[80] Debiasi E, Gajo A, Zonta D. On the seismic response of shallow-buried rectangular structures. Tunn Undergr Sp Technol 2013;38:99–113.
[81] Tsinidis G, Rovithis E, Pitilakis K, Chazelas JL. Seismic response of box-type tunnels in soft soil: experimental and numerical investigation. Tunn Undergr Sp Technol 2016;59:199–214.
[82] Li W, Chen Q. Effect of vertical ground motions and overburden depth on the seismic responses of large underground structures. Eng Struct 2020;205:110073.
[83] Wu W, Ge S, Yuan Y, Ding W, Anastasopoulos I. Seismic response of subway station in soft soil: shaking table testing versus numerical analysis. Tunn Undergr Sp Technol 2020;100:103389.
[84] Wu W, Ge S, Yuan Y. Seismic response characteristics of cross interchange metro stations: transversal response of the three-storey section. Eng Struct 2022;252:113525.
[85] JT/T4-2019. Laminated Bearing for Highway Bridge. Beijing, China: [37] Ministry of Transport of the People's Republic of China: 2019.
[86] Sadiq S, van Nguyen Q, Jung H, Park D. Effect of flexibility ratio on seismic response of cut-and-cover box tunnel. Adv Civ Eng 2019:1–16.
[87] Qiu D, Chen J, Cao X. Study on the seismic control measure of the underground large-scale frame structure. Structures 2022;40:328–43. https://doi.org/10.1016/j.istruc.2022.04.030.
[88] Tsinidis G. Response characteristics of rectangular tunnels in soft soil subjected to transversal ground shaking. Tunn Undergr Sp Technol 2017;62:1–22. https://doi.org/10.1016/j.tust.2016.11.003.
[89] Zhuang H, Zhao C, Chen Su, Fu J, Zhao K, Chen G. Seismic performance of underground subway station with sliding between column and longitudinal beam. Tunn Undergr Space Technol 2020;102:103439.
[90] Nriesdr. National research institute for earth science and disaster resilience. Natl Res Inst Earth Sci Disaster Resil 2019.
[91] Li T, Yang Y, Dai K, Ge Q, Wang J. Influence of ground motion duration on seismic performance of RC frame isolated by high damping rubber bearings. Eng Struct 2022;262:114398.
[92] Pang R, Chen K, Fan Q, Xu B. Stochastic ground motion simulation and seismic damage performance assessment of a 3-D subway station structure based on stochastic dynamic and probabilistic analysis. Tunn Undergr Sp Technol 2022;126:104568.
[93] Pang R, Zhou Y, Chen G, Jing M, Yang D. Stochastic mainshock-aftershock simulation and its applications in dynamic reliability of structural systems via DPIM. J Eng Mech 2023;149:4022096.
[94] Chengshun X, Zigang X, Xiu-li DU. Comparative study of simplified methods for seismic analysis of underground structure. Earthq Eng Eng Dyn 2017;37:65–80.
[95] GB 20688.4-2007. Rubber bearings-Part 4: Normal rubber bearings. Standardization Administration of China; 2007.